2020

Applied Laser Absorption Spectroscopy for Sensing in Detonative Flows

Kyle Thurmond
University of Central Florida

APPLIED LASER ABSORPTION SPECTROSCOPY FOR DETONATIVE FLOWS

by

KYLE D. THURMOND
B.S. University of Central Florida, 2013
M.S. University of Central Florida, 2016

A dissertation submitted in partial fulfillment of the requirements
for the degree of Doctor of Philosophy
in the Department of Mechanical and Aerospace Engineering
in the College of Engineering and Computer Science
at the University of Central Florida
Orlando, Florida

Fall Term
2020

Major Professor: Subith S. Vasu

ABSTRACT

A great deal of interest lies in detonative combustion due to its destructive potential and the theoretical thermodynamic advantages over traditional deflagration devices used for propulsion and energy. High energy materials and explosives combustion products and temperature must be characterized to gain greater insight into the energy release mechanisms, allowing for more tailored deployment. Predictive models for detonations employ various types of state equations, and temperature can be used as a check on the equation validity. However, the extreme environment of explosives is incredibly challenging to evaluate temperature. Additionally, these reactions are extremely fast, taking place over microseconds, and have an extremely large dynamic range, with pressures and temperatures exceeding 30 bar and 3000 K, respectively. For harnessing detonations for energy and propulsion, rotating detonation engines (RDEs) have received much attention due to their simple design and ability to be fed continuously. Many of the same challenges faced in characterizing explosive detonation are encountered in the flowfield of RDEs. These devices require fast measurements (MHz) in extreme environments, which allow the development of better models. The work discussed in this dissertation presents the development and demonstration of laser absorption spectroscopy (LAS) sensors for the characterization of detonative flows in an RDE and high-explosive material's fireballs. The development cycle is discussed, including selecting the target gases, line selection, system design, validation, and demonstration. Temperature and H_2O measurements within the detonation channel of a CH_4/Air fired RDE are presented, which show incomplete detonation combustion and a secondary combustion mode from unreacted products.

To my loving wife, Stephi, who inspires and fulfills me.

TABLE OF CONTENTS

LIST OF FIGURES

LIST OF TABLES

CHAPTER 1: INTRODUCTION

Motivation

Detonations are a mode of combustion where a supersonic exothermic reaction accelerates a shock wave. Interest in detonations lies in both its destruction potential and non-destructive applications. High energy materials and explosives have been used for their destructive power since the 10th century, when Chinese alchemists discovered black powder and used it in warfare. More advanced and higher energy materials have emerged since then, and a desire to better understand the detonation process so it may be used in a more targeted and controlled manner. How this chaotic force may be harnessed for energy may be less obvious. While deflagration occurs at roughly constant pressure, detonation may be approximated as a constant volume process that increases total pressure. This pressure gain can be harnessed to boost the energy efficiency of power and propulsion systems. The detonation process also has a shorter residence time, which results in lower production of undesired products such as NOx. Furthermore, the fast (supersonic) burning rates of detonations allow for smaller, potentially lighter hardware.

Proper characterization of temperature and combustion products is required to understand better the energy release of high energy materials and explosives. However, such measurements are considerably difficult. The evolution of the reaction takes place over a period of microseconds, requiring high-speed diagnostics. Additionally, the instrumentation must be able to handle large dynamic ranges and extreme conditions. For gram scale experiments, pressure may exceed 30 bar and temperatures in excess of 3000K. Developing instrumentation that is sensitive over such ranges and can handle such extremes is very challenging.

Rotating Detonation Engines (RDEs) have been subject to an increased interest in the last decade due to the thermodynamic advantages gained through detonative combustion, their compact size, and high flow potential. This technology intends to employ a detonation for releasing chemical energy, which produces a shock that is accelerated by a supersonic reaction zone resulting in higher density and pressures than in deflagration combustion. The promise of pressure gain technologies is increased efficiency with lower emissions for power and propulsion systems. Pressure gain systems have been proposed in various configurations, with the Pulse Detonation Engines (PDEs) having received the most significant amount of research. However, RDEs offer the advantages of operating at much higher frequencies (by one to two orders of magnitude), and detonation is initiated only once (continuous detonation). These factors make RDEs simpler in design, produce a more continuous power output, and more compact.

Advanced diode laser absorption spectroscopy-based sensors have become the go-to method for resolving harsh and fast-reacting flow thermodynamic properties. These techniques are now being turned to for understanding the complex process involved in an RDE cycle. Goldstein et al. developed a two-color tunable diode laser absorption spectroscopy (TDLAS) sensor for evaluating water temperature in an RDE [1]. This sensor used scanned-wavelength-modulation spectroscopy with second-harmonic detection (scanned-WMS-2f/1f), which achieved a bandwidth of 25kHz. The sensor was used to probe the throat of a converging-diverging nozzle at the exit of an RDE and capture temperature fluctuations at the engine's frequency (3.25kHz). Rein et al. utilized a MEMS-tunable Vertical-Cavity Surface-Emitting laser to capture transient water temperature at a bandwidth of 100kHz [2, 3]. This was used to probe the engine at multiple locations along its axis in the combustion chamber channel. The findings agreed with previous

modeling efforts, which showed a large spike in temperature followed by a gradual decline in the upstream location but a much less extreme behavior at the downstream location.

Organization of Dissertation

This dissertation presents the design and characterization of laser absorption sensors for measuring time-resolved combustion products and temperature within detonative flows. The document is organized as follows:

2) **Chapter 2** describes in detail the physics of light-matter interaction and the basis of laser absorption spectroscopy. The Beer-Lambert law is broken down into its components, laying the foundation for later chapters. Line shape functions, such as the Voigt and Galatry function, are discussed. Finally, the theory behind two-color thermometry is laid out.
3) **Chapter 3** discusses various laser absorption spectroscopy techniques, including fixed-wavelength, direct absorption (fixed-DAS), scanned-wavelength, direct absorption (scanned-DAS), and wavelength-modulation-spectroscopy (WMS). The advantages and disadvantages of each technique are outlined.
4) **Chapter 4** discusses the different test facilities that are used to evaluate and support the development of laser absorption spectroscopy instrumentation. High-temperature gas cells provide an ideal environment with minimal uncertainty and long sampling periods but are limited to temperatures below 1100 K. Shock tubes can generate high pressures and temperatures but are limited in gas composition and test time. Finally, flat flame burners provide an ideal combustion environment with a nearly uniform temperature distribution.

These burners can reach temperatures between 1800 to 2600 K and can be doped with different compounds.

5) **Chapter 5** discusses the characterization of NO in the mid-infrared region around 5.2μm using a shock tube and scanned wavelength, direct absorption technique. The line selection process is discussed, which identifies a transition that maximizes sensitivity in the temperature range of the measurements and minimizes interference from other species. Scanned measurements of NO in different bath gases are made over the temperature of 700 to 2100 K. A Voigt and Galatry function is fit to the scanned measurements allowing the linestrength and collisional half-width to be extracted.
6) **Chapter 6** discusses the design and challenges of practical sensing in combustion devices and test facilities. Challenges include making the instrumentation semi-portable, making measurements outside, dealing with extreme environments, handling vibrations and acoustics, and coupling to the test facility.
7) **Chapter 7** discusses temperature and H_2O measurements within the detonation channel of a rotating detonation engine (RDE). The CH_4-Air fired Aerojet-Rocketdyne designed RDE, and testing took place at the University of Alabama. Results show incomplete detonation combustion, which led to a secondary combustion mode, initiated by the trailing oblique shock.

CHAPTER 2: FUNDAMENTALS OF ABSORPTION SPECTROSCOPY

Beer-Lambert Law

Fundamental to absorption spectroscopy is the Beer-Lambert law (equation 1), which describes monochromatic light absorption by a given molecule. Here, I_0 and I_t are the incident and transmitted light, respectively, S is the line strength (cm^{-2}/atm), ϕ (cm) is the transmission line shape, P_i (atm) is the partial pressure, and L (cm) is the path length.

$$\alpha_\nu = \ln\left(\frac{I_\nu}{I_{\nu,0}}\right) = -S_i(T)\phi_\nu P x_i L, \tag{1}$$

The absorbance, α_ν, is shown in Figure 1 for several molecules of interest in combustion studies, including CO_2, CO, and H_2O. The absorption spectra were simulated using the HITRAN 2016 database [4], which provides a compilation of spectroscopic parameters to predict and simulate light transmission in the atmosphere.

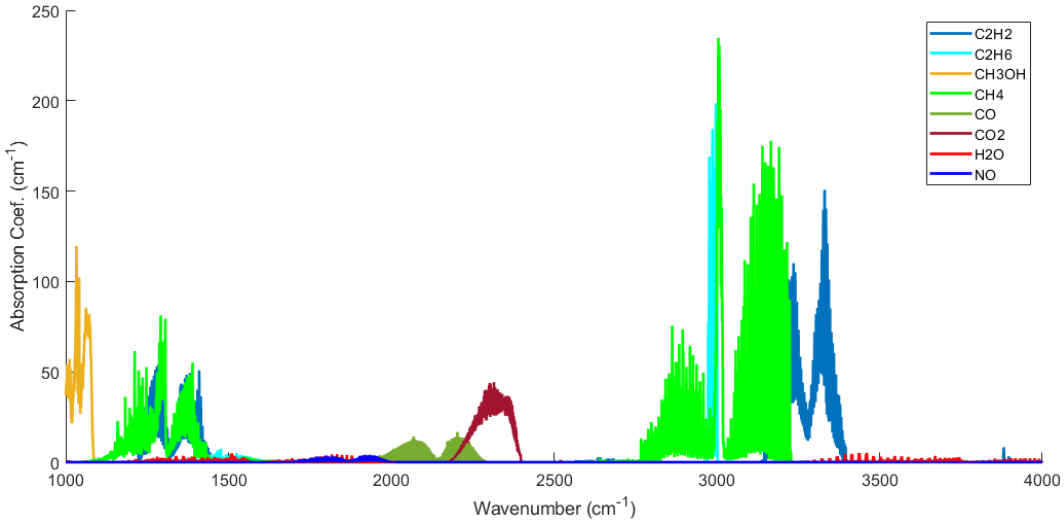

Figure 1: Absorption spectra of common species of interest in the mid-infrared region. Simulated using HITRAN database [4].

The line shape function ϕ_ν is approximated with a Voigt function for collisional and Doppler-broadened transitions. The lineshape is normalized to have a unit area across the line, so the integrated absorbance is:

$$A_i = \int \alpha_\nu d\nu = S_i(T) P x_i L \tag{2}$$

The linestrength scales with temperature as follows:

$$S(T) = S(T_0)\frac{Q(T)}{Q(T_0)}\left(\frac{T_0}{T}\right)\exp\left[-\frac{hcE''}{k}\left(\frac{1}{T}-\frac{1}{T_0}\right)\right]\left[1-\exp\left(\frac{-hc\nu_0}{kT}\right)\right]\left[1-\exp\left(\frac{-hc\nu_0}{kT_0}\right)\right]^{-1} \tag{3}$$

where $Q(T)$ is the partition function, E'' [cm^{-1}] is the lower-state energy, ν_0 [cm^{-1}] is the line-center frequency, h is Planck's constant, c is the speed of light, and k is Boltzmann's constant.

Linestrength and Lower-State-Energy

Linestrength may be inferred by spectrally resolving a line at multiple temperatures and integrating it to produce the integrated absorbance (equation 2). This data can be fitted to equation 3, with the room temperature line strength, $S(T_0)$, and lower state energy, E'', as unconstrained variables. Similarly, $S(T_0)$ may be determined by measuring integrated absorbance at T_0 and multiple pressures, leaving only E'' unconstrained.

Linestrength and lower state energy are generally well characterized in databases for stronger features, but weaker lines become more prominent as temperatures increase. These weaker lines are poorly resolved or missing in spectroscopic databases. Resolving this data is critical for instruments design for very high temperatures and moderate pressures.

Line Shifting Mechanisms

The line center, ν_0, of the transition is influenced by temperature and pressure, which is a response to changes to intermolecular potential and, correspondingly, changes in molecular spacing. Change in the line center due to pressure shifting, $\Delta\nu_{0,P}$ [cm^{-1}], is modeled using the pressure-shift coefficient, δ_i [cm^{-1}/atm], and partial pressure, P_i [atm], for each collisional partner, as shown in equation 4.

$$\Delta\nu_{0,P} = \nu_{0,P} - \nu_0 = \sum P_i \delta_i \tag{4}$$

The pressure-shift coefficient is temperature dependent, which is modeled using a power-law function, as shown in equation 5.

$$\delta_i(T) = \delta_i(T_0)\left(\frac{T_0}{T}\right)^m \tag{5}$$

The optical frequency will see a Doppler shift if there is a bulk gas speed component, u_b [cm/s], in the direction of the photon. The shift in the line center, $\Delta\nu_{0,D}$ [cm^{-1}], is described by equation 6.

$$\Delta\nu_{0,D} = \nu_0 \frac{u_b}{c} \tag{6}$$

Line Shape Functions

A simple harmonic oscillator model of a molecule would suggest that resonance occurs at discrete frequencies. However, in real systems, transitions are broadened by thermal motion and collisions. The line shape function is a probability function of a transition describing how

absorbance is distributed over frequency space. There are many line shape models that vary in complexity and robustness. The most commonly employed is the Voigt function, which several computationally efficient estimations have been developed and are considered accurate in most combustion relevant conditions [5-7]. Another commonly employed function is the Galatry function, which accounts for collisional (Dicke's) narrowing. The parameters to model the line shape for a given transition of a given molecule using the Voigt function are available in databases such as HITRAN and HITEMP. However, these databases were built on air measurements and may be missing information relevant to higher temperatures. Figure 2 shows scanned measurements of 2.87% NO in N_2 compared with simulations using the HITEMP database (NO in air). The difference in bath gas resulted in a large deviation, particularly near the line center. Therefore, characterizing a feature in a combustion relevant environment is critical in developing a practical diagnostics instrument.

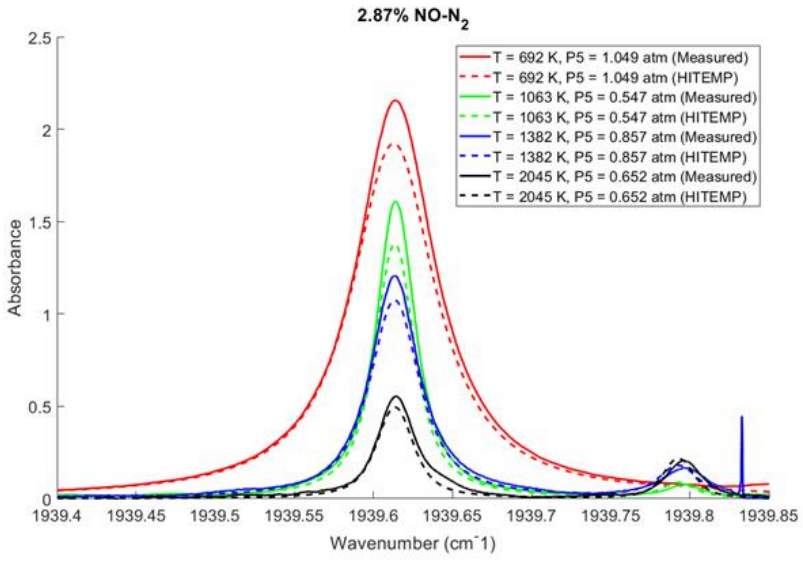

Figure 2: Comparison of measured NO absorbance in N_2 and simulated NO in air using the HITEMP database [8].

The Gaussian profile accounts for Doppler broadening, resulting from the absorbing molecules' random thermal motion, which causes a transition to broaden about its line center. Therefore, the Gaussian profile should be used at high temperatures or very low pressures. The Gaussian profile is given by equation 7.

$$\phi_D(\nu) = \frac{2}{\Delta\nu_D}\left(\frac{\ln 2}{\pi}\right)\exp\left[4\ln 2\left(\frac{\nu-\nu_0}{\Delta\nu_D}\right)^2\right] \tag{7}$$

The Doppler full-width at half-maximum (FWHM), $\Delta\nu_D$ [cm^{-1}], for a Maxwellian velocity distribution is given by equation 8.

$$\Delta\nu_D = 2\sqrt{\ln 2}\,\Delta\nu_D' = 7.1623\times10^{-7}\nu_o\sqrt{\frac{T}{M}} \tag{8}$$

Here $\Delta\nu_D'$ [cm^{-1}] is the 1/e Doppler half-width at half-maximum (HWHM), and M [g/mol] is the molecular weight of the molecule.

The Lorentzian profile accounts for collisional broadening. As molecules collide, they transfer energy to the different modes, resulting in uncertainty in the energy level. The Lorentzian profile may be used in cases of very low temperatures—it is given by equation 9.

$$\phi_L(\nu) = \frac{1}{2\pi}\frac{\Delta\nu_C}{(\nu-\nu_0)^2+\left(\frac{\Delta\nu_C}{2}\right)^2} \tag{9}$$

The collisional FWHM, $\Delta\nu_C$ [cm^{-1}], is given by equation 10, with X_i being the mole fraction and γ_i [cm^{-1}] is the broadening coefficient of collisional partner i.

$$\Delta\nu_C(\nu) = 2P\sum X_i\gamma_i(T) \tag{10}$$

The broadening coefficient is temperature-dependent and is typically modeled using a power law shown in equation 11.

$$\gamma_i(T) = \gamma_i(T_0)\left(\frac{T_0}{T}\right)^n \tag{11}$$

The Voigt profile is a convolution of the Lorentzian and Gaussian profiles, accounting for both doppler and collisional broadening. As such, it is given by equation 12.

$$\phi_V(x,y) = \frac{y}{\pi}\int_{-\infty}^{+\infty} d\zeta \frac{\exp(-\zeta^2)}{y^2 + (x-\zeta)^2} \tag{12}$$

Here, $x = (\nu - \nu_0)/\Delta_D'$ is the normalized relative line center frequency and $y = P\gamma/\Delta\nu_D'$ is the normalized collisional broadening. In practice, equation 12 is not used but, instead, the numerical approximation developed due to the large computation toll [5-7].

Two-Color Thermometry

Taking the ratio (R) of the integrated absorption of the two different features results in a function of temperature only.

$$R = \frac{A_1}{A_2} = \frac{S_1(T)}{S_2(T)} = f(T), \tag{13}$$

Forming this function and differentiating with respect to temperatures yields the temperature sensitivity, ζ, which is important in considering the selection of transitions to use for temperature measurements.

$$\zeta = \frac{\mathrm{h}c(E_1'' - E_2'')}{kT}, \tag{14}$$

This shows that the lower energy state, E'', of the two selected transitions determines the sensitivity of thermometry.

Summary

Laser absorption spectroscopy is a powerful technique that can non-intrusively evaluate gas composition, temperature, pressure, and velocity. The foundation of LAS is the Beer-Lambert law, which relates the fraction transmittance of light through matter. By directly measuring the fraction transmittance, the mole fraction of an absorbance molecule can be inferred. If the absorbance of a molecule is measured at multiple wavelengths, the temperature can be evaluated from their ratio. By measuring the Doppler shift, as described in equation 6, the bulk gas speed can be measured. Finally, by measuring collisional broadening and comparing it with high-fidelity simulations, pressure can be measured.

CHAPTER 3: ABSORPTION SPECTROSCOPY TECHNIQUES

Introduction

This chapter discusses the most prevalent laser absorption spectroscopy (LAS) techniques employed in combustion diagnostics experiments. Two primary categories exist, direct absorption (DA) and wavelength modulation spectroscopy (WMS). Further division can be made into fixed wavelength and scanned wavelength. In fixed wavelength techniques, the laser's wavelength is held at a resonant frequency with the analyte, while with scanned wavelength, the wavelength is scanned across an absorbing feature. Either approach can employ DA, where the laser's wavelength is held or scanned at a constant rate, or WMS, where the wavelength is simultaneously sinusoidally modulated with time. Each approach has its advantages, which are discussed in detail in this chapter.

Fixed-Wavelength, Direct Absorption

In principle, fixed-wavelength, direct absorption (fixed-DA) is the most straightforward LAS technique as the laser's wavelength and intensity are held constant. Fixed-DA allows for high-speed measurements, usually limited by DAQ sampling rate or detector speeds (MHz). Typically, wavelengths are selected that give the right amount of sensitivity for the expected environment and pathlength while minimizing interference from other products. However, this technique has no means of retaining baseline information (non-resonant losses), rejecting low-frequency noise, and requires accurate spectral characterization of the analyte in operating conditions. Since the laser's wavelength is fixed at some resonance frequency of the analyte, any changes in the baseline due to emission or non-resonant losses (soot, window fowling) are difficult or impossible to detect.

Additionally, since the wavelength is held constant, no spectral information may be extracted. Significant uncertainties may occur from inaccurate modulating of the gas spectra (from pressure shifts or line strength data) or uncertainty in the laser's wavelength. Another challenge with fixed-DA is in demultiplexing wavelengths. It is desirable to combine multiple wavelengths into a single beam so that simultaneous measurements may occur across a common path. While not the only means of accomplishing this, demultiplexing typically employs diffraction gratings. This is a problematic approach that requires significant space and is prone to various forms of noise, which is expanded on further in chapter 6. Figure 3 shows raw data for fixed-DAS measurements of a shock heated non-reactive mixture of CO. As the pressure and temperature changes, the absorbance of the laser changes.

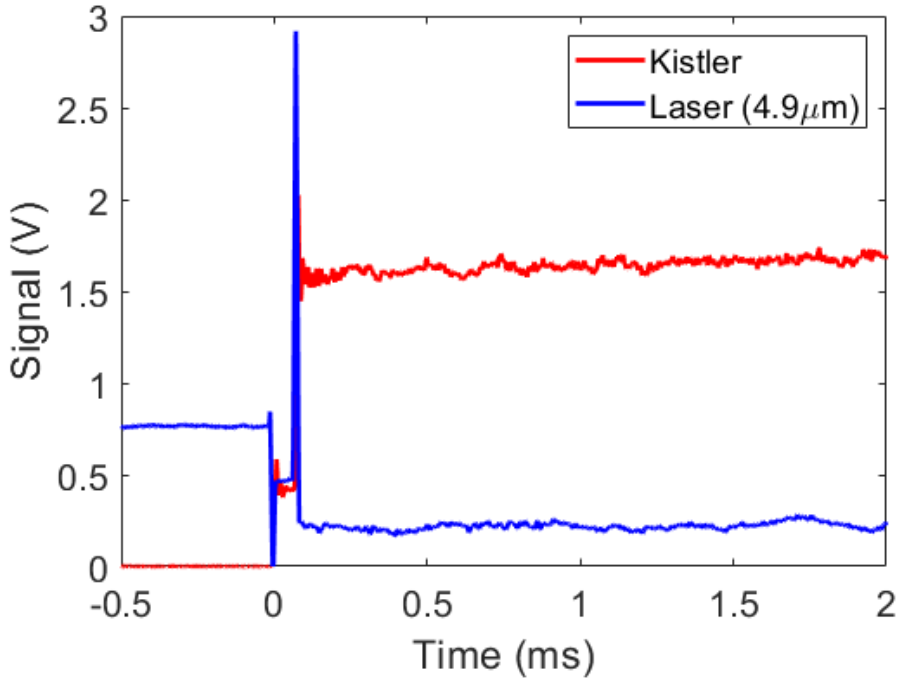

Figure 3: Raw data for fixed-DAS measurements of shock heated CO (0.1%) in Ar. Reflected shock temperature was 1210 K and pressure was 9.98 atm.

Scanned-Wavelength, Direct Absorption

Scanned-wavelength, direct absorption (scanned-DA) sweeps the laser's wavelength over time to provide increased spectral information. This approach reduces wavelength uncertainty and the burden for high-fidelity simulations of the analyte's absorbance spectra. A central wavelength may be locked to a known feature, allowing synchronizing simulation data with measurements. Furthermore, by fully scanning over an absorption feature, the integrated absorbance may be obtained, eliminating unknowns from broadening parameters. Figure 4 shows raw data for scanned measurements of shock heated H_2O using two wavelengths near 2.5μm. The laser intensity and wavelength are coupled, so as the laser frequency decreases, the intensity increases. An etalon is used to track the relative change optical frequency of the lasers.

By scanning the laser off of any resonant features, baseline corrections are possible. While there is no absorption, emission, or non-resonant losses may be evaluated. If multiple absorption features can be scanned, the measurement's dynamic range and uncertainty can be significantly improved. Hyperspectral direct absorption is an emerging subcategory of scanned-DA, where the laser's wavelength is scanned over $10cm^{-1}$ at fast rates (> 10kHz). While this technique is very simple and provides more information than fixed-DA, scanning the laser comes at the cost of bandwidth. Scanning the wavelength is typically limited to rates less than the time scales of fast combustion processes. Furthermore, though this technique is more robust than fixed-DA, it can still suffer from low SNR.

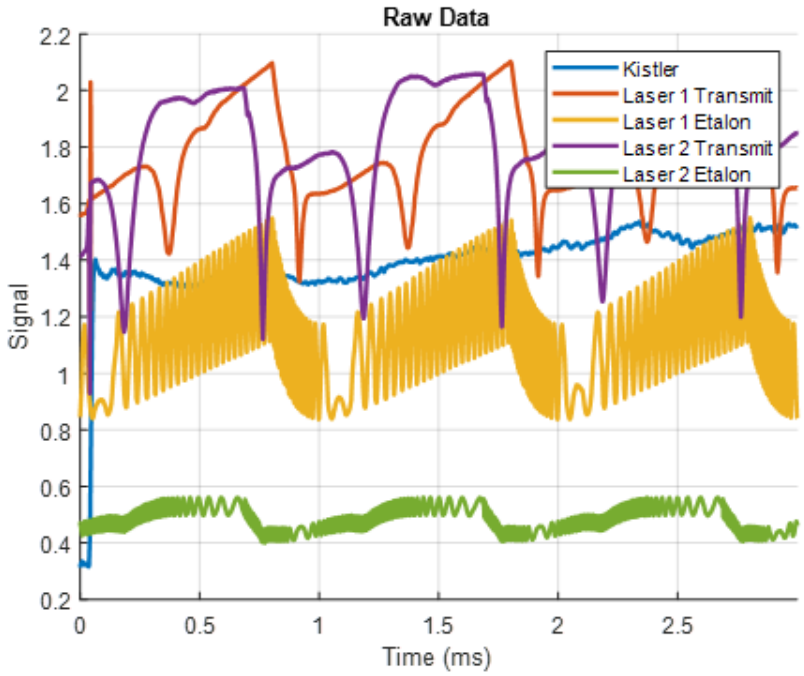

Figure 4: Example of scanned wavelength, direct absorption measurements. Two lasers are scanned over to spectral regions to measure H_2O and temperature. An etalon is used to track relative wavelength change (gold and green signals).

Wavelength-Modulation-Spectroscopy

By modulating the wavelength about a fixed point on an absorption feature, fixed-WMS shifts the measurements to the modulated frequency, f, and harmonics. This elevates the signal above low-frequency noise attributed to the laser, detectors, and the environment, greatly improving SNR. The signal is extracted from the detector signal through a lock-in amplifier. This technique may be further enhanced by normalizing higher harmonics by the first harmonic (WMS-nf/1f), which removes the DC component from the signal, eliminating effects from beam steering or window fouling. Figure 5 shows the Fourier space for a fixed-WMS signal modulated at 50kHz. Like the fixed-DA technique, this approach lacks spectral information, which produces uncertainty carried over from unknowns in gas models or wavelength drift in the laser.

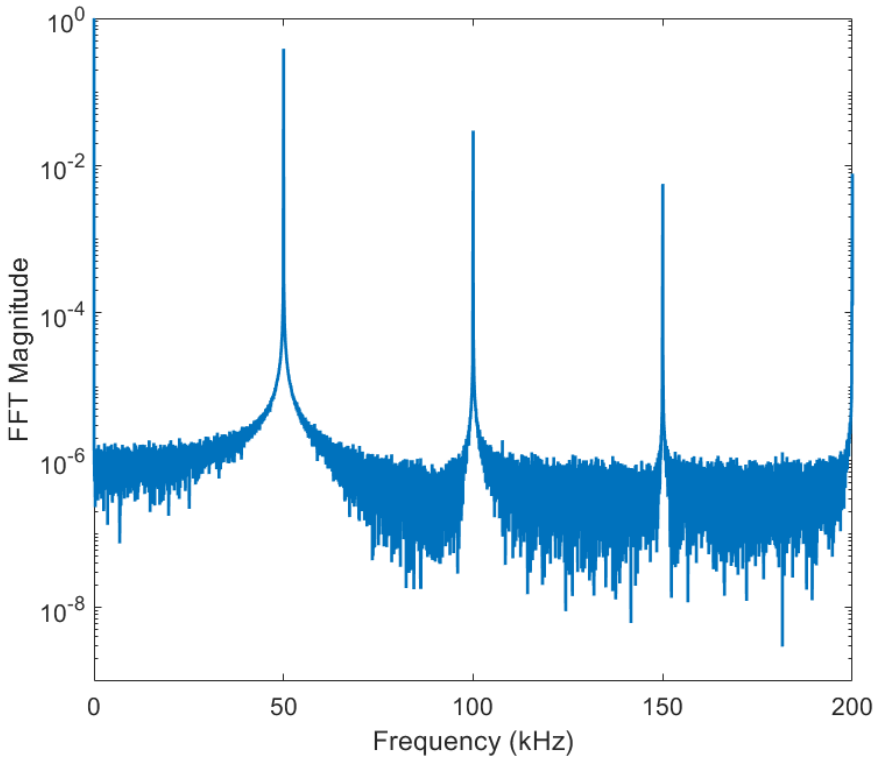

Figure 5: FFT of simulated transmitted light for fixed-WMS through a water feature around 2.55μm. The modulation frequency is at 50kHz.

Scanned, Wavelength-Modulation-Spectroscopy

Scanned-WMS imposes a fast modulation over a slower scan rate, combining the benefits of scanned-DA with WMS. Scanning the laser allows for spectral fitting, eliminating the need for knowledge of broadening and pressure shift information. Figure 6 shows the Fourier space for a scanned-WMS signal modulated at 50kHz and scanned at 7kHz. While scanned-WMS is a powerful technique that provides the lowest uncertainties, it is also the most complex due, in part, to the increased frequency information. The sideband clustered around the harmonics describes how the WMS-n*f* changes as it is scanned across the absorption features.

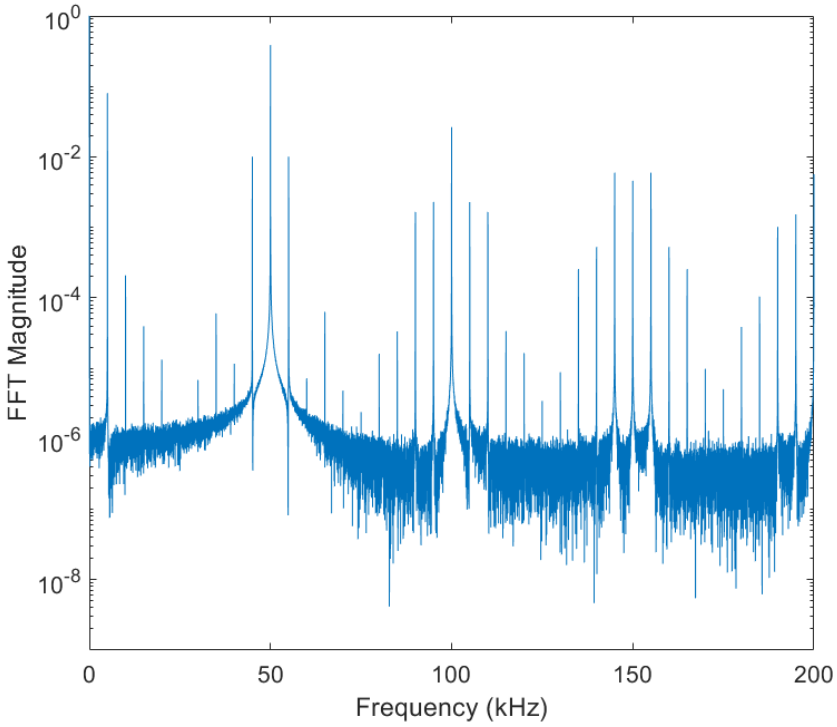

Figure 6: FFT of simulated transmitted light for scanned-WMS through a water feature around 2.55μm. The modulation frequency is at 50kHz, with a scan rate of 7kHz.

CHAPTER 4: EXPERIMENTAL FACILITIES

Introduction

The following presents a discussion of the three technologies used to extract gas spectral data in combustion studies. The discussion is meant to point out each technology's strengths and weaknesses and how they are best used. It is not necessarily an in-depth overview of the technologies and how specific challenges may be overcome.

Shock Tube

The shock tube provides the broadest access to temperature and pressures, as well as gas radicals, but it comes with a few challenges and a high data cost. The first challenge is the short test times, which are typically a few microseconds. This is generally an acceptable test time, allowing several scans over a line at low to moderate pressures. Still, it is desirable to do extended scans at slower rates (for high resolution) so that a broad spectrum of data may be resolved. Another challenge is the constraint on diluents used, as the gas mixture should have a specific heat ratio of ~5/3 to mitigate bifurcation. Typically, this is Ar, which is acceptable for shock tube diagnostics, but for instruments developed for combustion devices (propulsion, internal combustion engines, gas turbines, etc.), measurements are not relevant. The last point is the high cost of tests, with each measurement requiring a great deal of gas, including He, and limited to four to six conditions (T, P) a day.

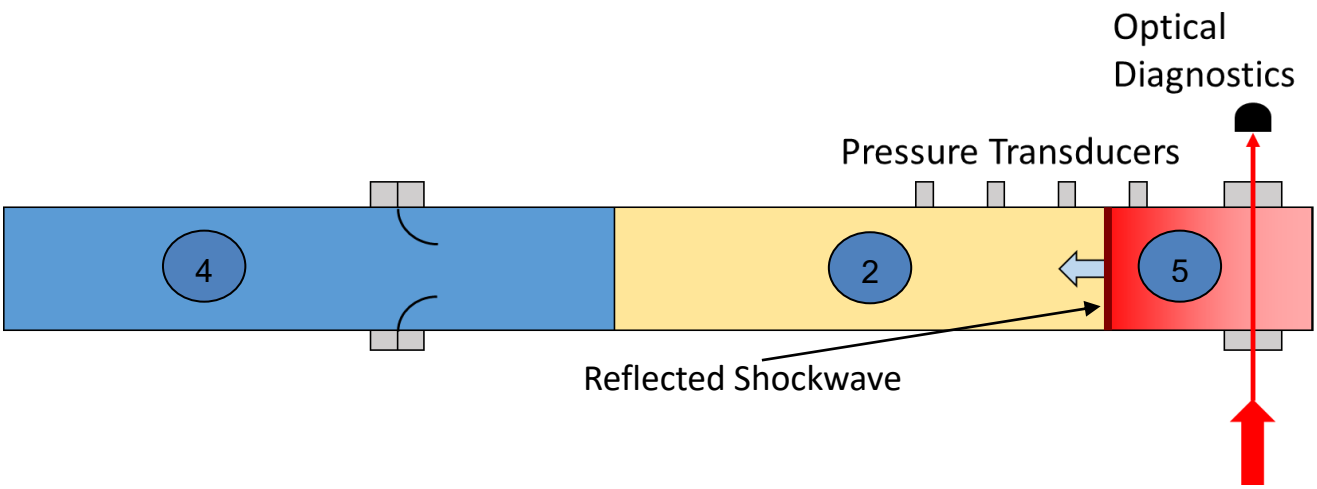

Figure 7: Operating diagram of a shock tube.

Given the abilities and limitations of the HPST, it should be used whenever high pressures are necessary and spectral range is limited to no more than a couple of wavenumbers. The shock tube could be used to extract line strength temperature dependence, but the FFB may better serve this since pressure variation is unnecessary. The shock tube provides a suitable method for extracting collisional data, but some work must be done to get around the diluent constraint. This has been done by Mulvihill et al. to extract He and O_2 broadening parameters for CO [9]. To achieve this, they first resolved broadening parameters for CO-Ar, then added He or O_2 and subtracted the broadening from Ar.

Flat Flame Burner

The flat flame burner (FFB) allows tests to high temperatures (up to 3500K) and is cheap and straightforward to operate, providing an extended testing time or high measurement volume. However, the FFB is generally limited to atmospheric conditions, and edge effects can present some challenges for line-of-sight measurements. Edge effects (boundary layers, non-homogeneous

line of sight) must be accounted for in post-processing, shown by Zhou et al. [10]. Additionally, there is limited control over broadening partners.

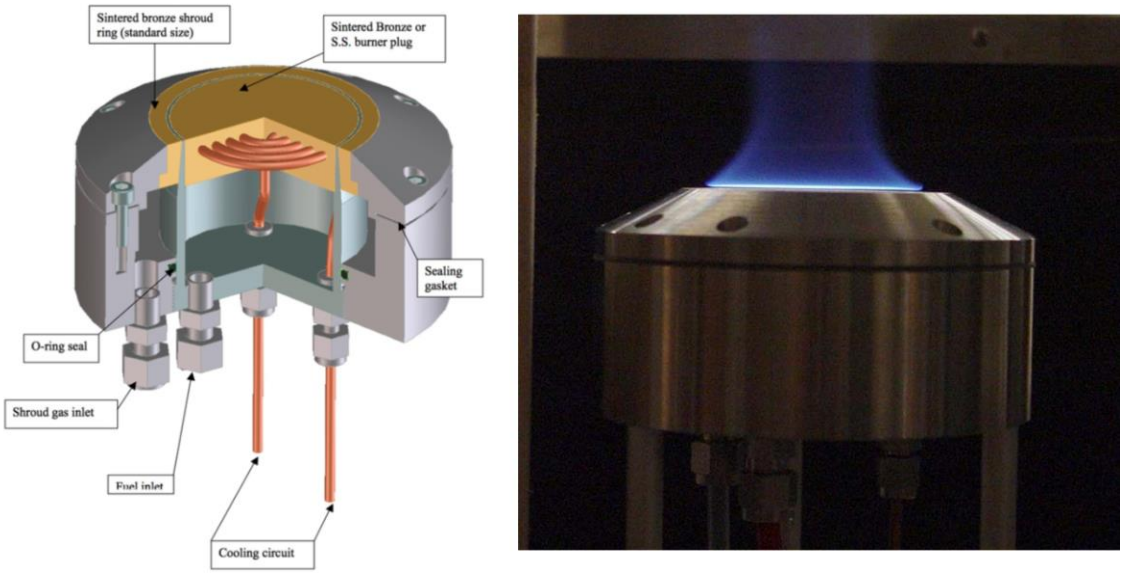

Figure 8: Schematic and photograph of the McKenna burner for static temperature measurement validation.

Long test times mean lower uncertainty and enable broad-spectrum measurements. Spectroscopic databases such as HITRAN and HITEMP generally provide accurate information on line strength and position of strong transitions, but data for weak lines may be inaccurate or missing. This information becomes crucial at very high temperatures. The FFB provides an excellent means of gathering information on line strength parameters, including temperature dependence and position. Rutkowski et al. used an FFB to identify line positions for water in the 6250-6670cm^{-1} region at 1950K [11]. It may be possible to extract broadening parameters at atmospheric conditions, but limited control of gas composition makes this challenging.

The FFB will best be served as a general validation test apparatus for TDLAS instruments in combustion environments. For measurements being made in air-breathing combustion devices, HITRAN/HITEMP may still be applicable as it provides self-broadening and air-broadening terms. The FFB allows the validation of this data very easily and with minimal time demand. Similarly, calibration curves and expanded spectral data relevant to combustion environments can easily be checked in a range of conditions (variation in equivalence ratio or fuel).

High-Temperature Gas Cell

The high-temperature gas cell would allow for limited temperature (<1030K) and spectral access (0.2-8μm) but broad pressure (vacuum-200bar), extended test times, and high control of gas composition. The challenges of the HTGC are primarily in its construction, which limits its temperature range due to metal fatigue. While ~1000K is the typical limit for metal gas cells, there are examples of constructions that can handle temperatures up to 1200K [12].

The HTGC would greatly compliment the HPST, allowing for linestrength extraction and broadening terms up to 1000K with much less effort and cost. The ability to precisely control the gas composition also provides a much better avenue for interrogating broadening parameters. Broadening parameters for self- and He- could be gathered using the HTGC used in boundary cases for extrapolating high-temperature terms using the HPST.

CHAPTER 5: SPECTROSCOPIC DATA MEASUREMENTS OF NO

Introduction

Nitric oxide (NO) is an undesirable product of combustion due to its contribution to ozone depletion, acid rain production, and high toxicity. For this reason, there is much interest in highly sensitive instruments for sensing NO in combustion products. Sensors that can measure spatial and transient formation at the parts-per-million (ppm) level is sought after in new combustion hardware designed to reduce NOx formation. NO also forms in significant quantities in CHNO compounds used in weapon and explosive systems, making it an attractive target for two-color thermometry.

Line Selection

For combustion devices, the major challenge is NO, and H_2O have significant spectral overlap, and the production of H_2O is about 10^4 times greater. Figure 9 mole fraction normalized absorption coefficient for NO and H_2O at combustion relevant conditions (2000 K, 5 atm) in the mid-infrared fundamental band. There are a few notable lines that appear to be suitable, but this plot can be misleading. As noted, the concentrations of NO and H_2O are significantly disproportionate. While NO may be around 10ppm, H_2O can be as has as 10%. At these concentrations, absorbance is on the order of 10^{-3} for NO, which is challenging enough resolve. The $^2\Pi_{3/2}$ R(20.5)($\nu = 1 \leftarrow 0$) around 1940cm^{-1} is relatively isolated. At elevated pressures (>2 atm), H_2O interference is unavoidable but nearly flat across the line's width. This makes scanned-WMS techniques suitable for measuring the minuscule absorbance while neglecting the baseline effect of the H_2O.

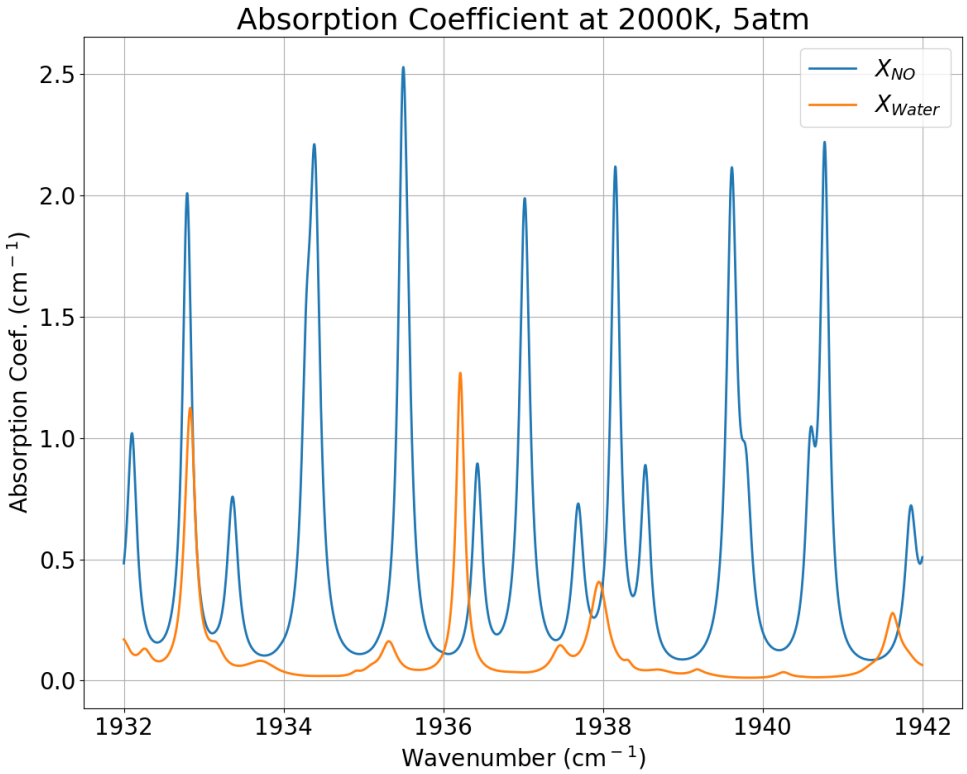

Figure 9: Possible nitric oxide (NO) absorption features near 5.2um at 2000K and 5 atm. Simulated using the HITEMP database [8].

Experimental Method

A shock tube with a 14.2cm inner diameter was used to shock heat mixtures of NO over temperature ranges 700 to 2100K, around 1 atm. Mixtures used included 2.87% NO in N_2 and 3.08% NO in CO_2. Since the parameters of interest are linear dependent on pressure, the pressure was kept low during the experiments to simplify data gathering. By keeping the pressure low, the lines remain narrow and can be thoroughly scanned. Additionally, low pressure reduces non-ideal effects in shock experiments, such as boundary layers build up.

Figure 10 shows a schematic depicting the optical arrangement on the shock tube, including laser, driving electronics, and detectors. A quantum cascade laser (QCL) from Alpes Lasers was

used to measure the absorption features. The laser was injection current tuned using a sawtooth function at a rate of 1kHz. A Wavelengths Electronics QCL 500 LAB A was used for current control, and a Wavelength Electronics LFI3751 was used to control the QCL temperature. Three Vigo Electronics mercury cadmium telluride (MCT) photovoltaic detectors were used to sample the laser along the beam path. An 8.3 cm silicon etalon was used to track relative wavelength during scanning. Finally, a Bristol 771B spectrometer was used to tune the laser to the desired center frequency. The laser was aligned through an optical port in the shock tube, which is 2 cm away from the end wall.

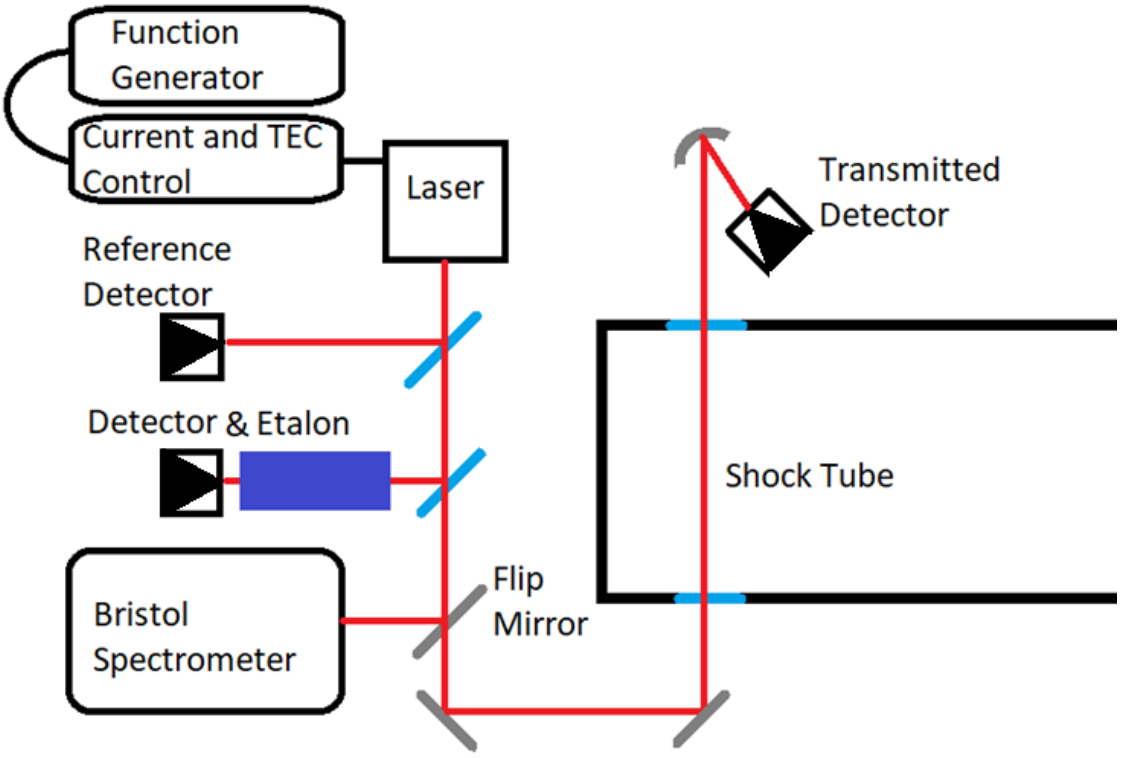

Figure 10: Laser setup for shock tube measurements of NO. The arrangement includes three MCT photovoltaic detectors, an 8.3 cm silicon etalon, and a Bristol spectrometer.

Figure 11 shows raw data of scanned measurements of a NO-N_2 mixture shock heated to 1215 K, which shows the signals for the lasers and pressure trace before and after the arrival of the shock wave. The incident shock arrives at time zero, then approximately 50μs later the reflected shock passes, increasing the pressure to just below 1 atm. Before the shock arrival, a narrow transition can be seen in the transmitted signal, which then significantly broadens. The blue trace represents the laser transmission through the etalon, which produces a fringe approximately every 0.017 cm^{-1}. By counting the fringes, the relative change in optical frequency can be tracked.

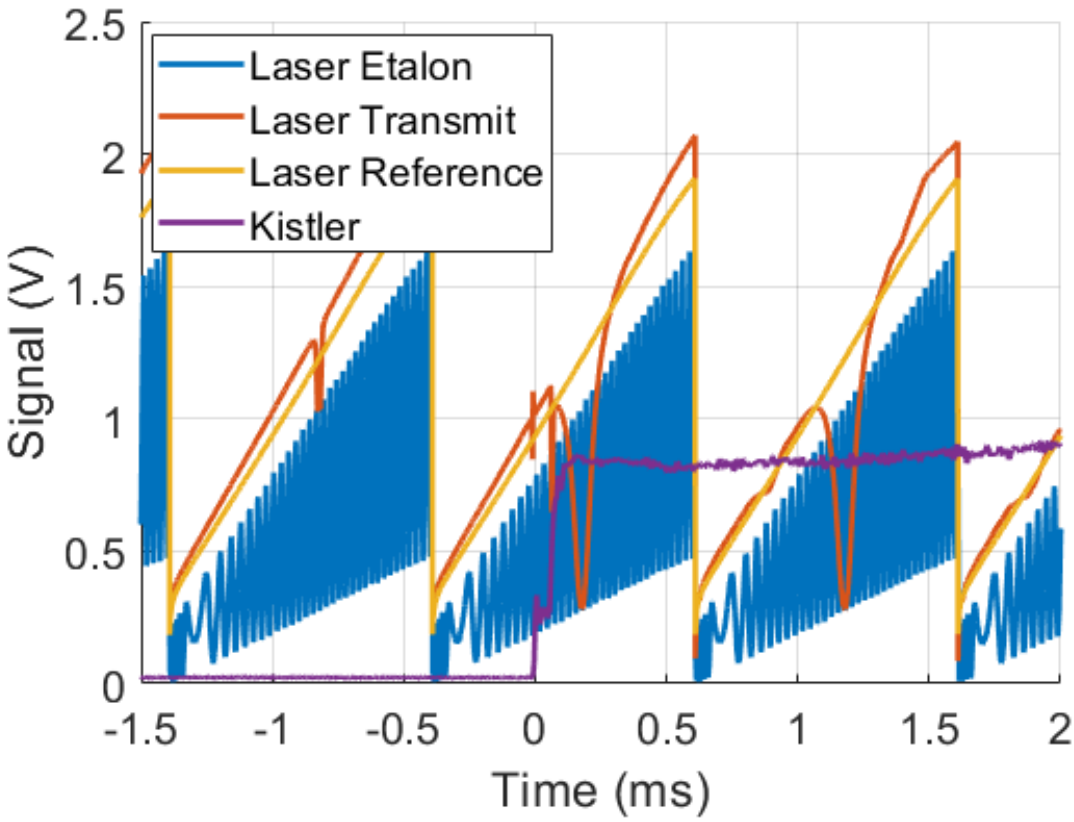

Figure 11: Raw data from scanned measurements of shock heated NO at 1215 K and 0.92 atm.

The laser was scanned over a range of approximately 0.5 cm^{-1}, which is sufficient to fully resolve the $^2\Pi_{3/2}$ R(20.5)($\nu = 1 \leftarrow 0$) and $^2\Pi_{1/2}$ R(20.5)($\nu = 1 \leftarrow 0$) lines, as shown in Figure 12 and Figure 13. A Voigt and Galatry profile was fit to data, which is also shown in the figures. In Figure 12, the measurement at 1215 K is shown, and, at this temperature, the $^2\Pi_{3/2}$ R(20.5)($\nu = 1 \leftarrow 0$) is considerably larger than the $^2\Pi_{1/2}$ R(20.5)($\nu = 1 \leftarrow 0$) line. However, in Figure 13, the lines are closer in value. The line pairs have much different temperature sensitivities (lower state energies), making them useful candidates for two-line thermometry.

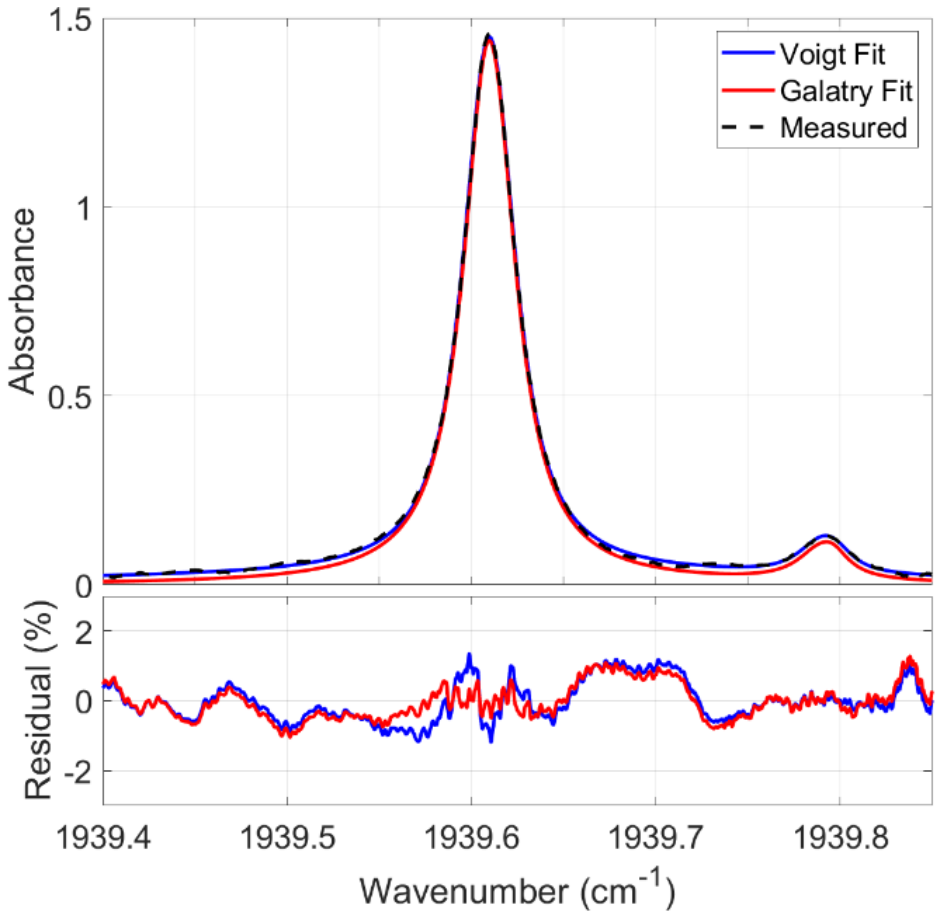

Figure 12: Shock heated NO (2.87%) in N2 at 1215 K, 0.71 atm.

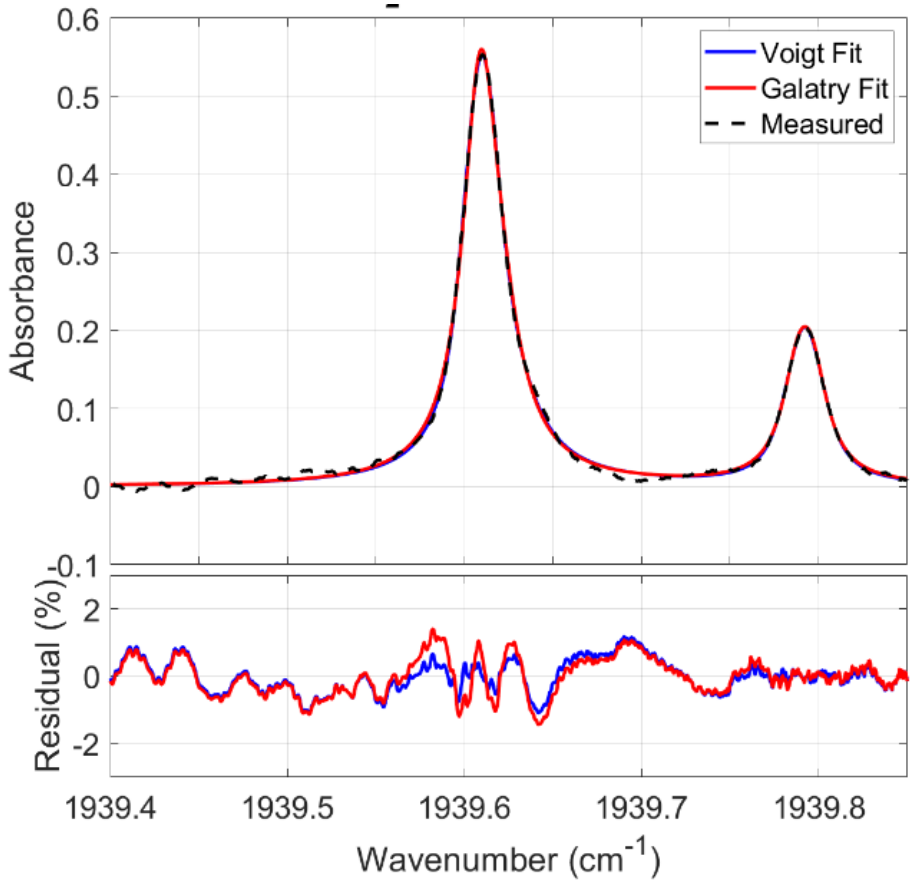

Figure 13: Shock heated NO (2.87%) in N_2 at 2045 K, 0.652 atm.

Figure 14 shows shock heated measurements of 3.08% NO in CO_2 at 1652K and lineshape fits (Voigt and Galatry). The CO_2 shocks contain more noise and uncertainty due to the non-idealities inherent in using CO_2 as a diluent in shock experiments. In particular, high CO_2 concentrations produce larger boundary layers and shock bifurcation. This produces a region of colder gases of unknown thickness. While this effect was reduced by using low pressures, it not avoidable when using high CO_2 concentrations. The bifurcation produces a gradient between these regions, which causes beam steering and noise in the laser. While the profile fits' residuals are not as good as the NO-N_2 shocks, they are still within 2% around the line peak.

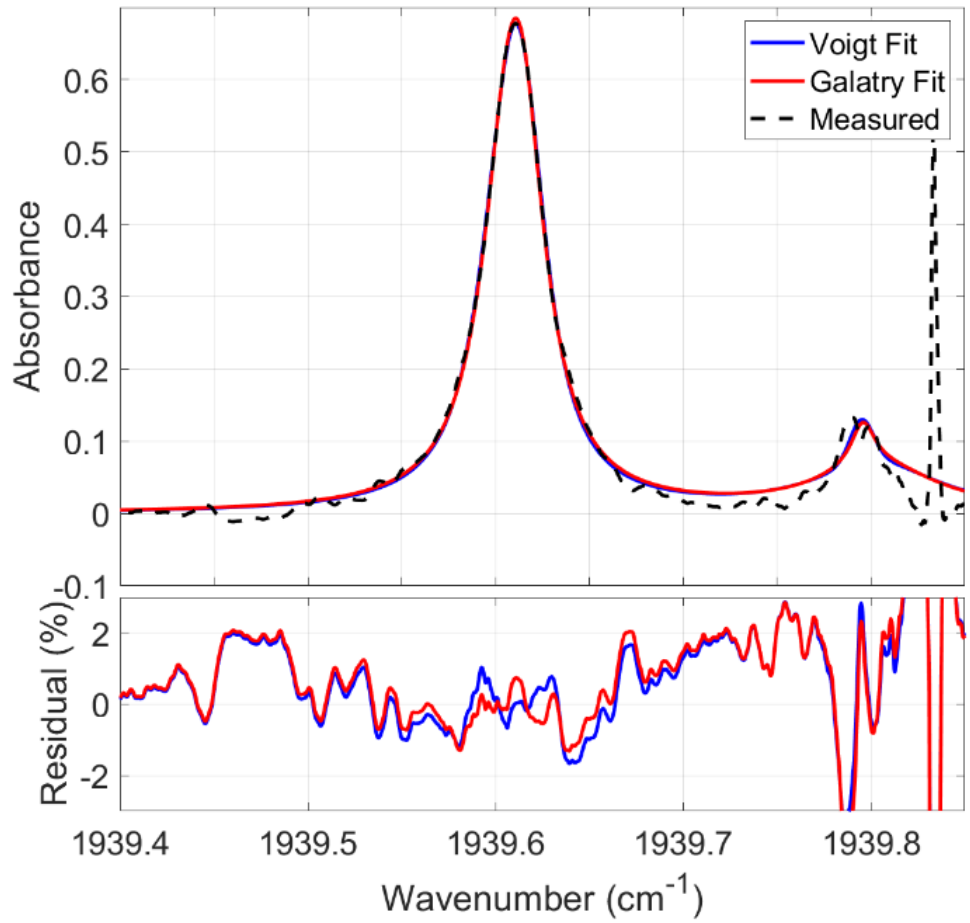

Figure 14: Shock heated NO (3.08%) in CO_2 at 1652 K, 0.681 atm.

Line Strength Measurements

From equation 5 in Chapter 2, two unknowns exist: the line strength at reference temperature, $S(T_0)$, and the lower state energy, E''. From equation 2 in Chapter 2, the line strength can be extracted by integrating the absorbance, so the line shape goes to unity, then dividing out the pressure, pathlength, and mole fraction. Figure 15 shows the integrated absorbance of the $^2\Pi_{3/2}$ R(20.5)($v = 1 \leftarrow 0$) at a temperature of 296 K between pressures 3 to 60 Torr. The transition actually has two features that can only be distinguished at low pressures, as shown on the right

side of Figure 15. At elevated pressures, this transition is considered one feature, and the line strengths are summed. From this plot, the slope is extracted and used to calculate $S(T_0)$.

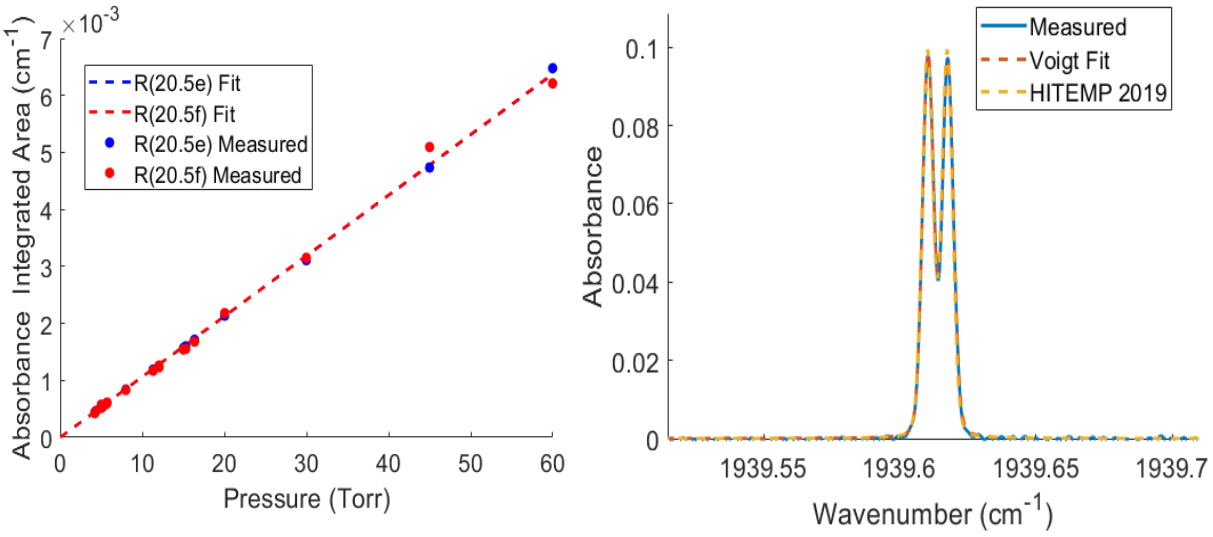

Figure 15: Linestrength measurements of NO at reference temperature, T_0.

Figure 16 shows the line strength measurements for the two NO lines from 700 to 2000 K, which is compared to HITEMP 2010 simulations. The line strength measurements were fit with an equation of the form shown in equation 3. The measured line strength at T_0 was found to be 0.3971 cm^{-2}/atm while HITEMP reports 0.3724 cm^{-2}/atm. The lower-state-energy, E'', was measured at 749.9 cm^{-1}, while HITEMP reports 735.4 cm^{-1}. The difference in measured values and values reported by HITEMP are within HITEMP's uncertainty (5-10%).

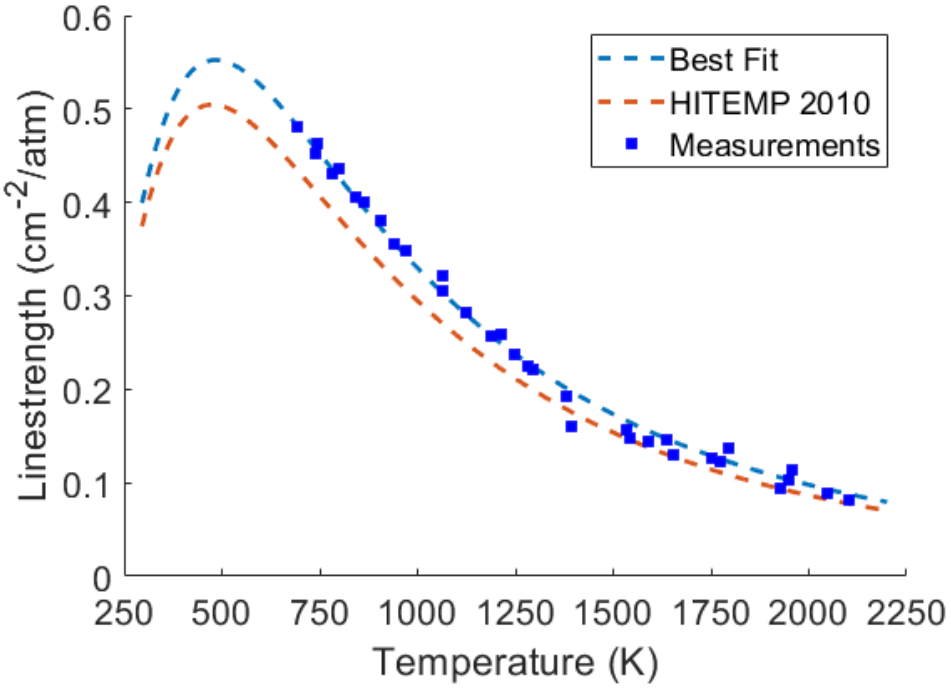

Figure 16: Lines strength measurement from shock heat NO measurements.

Line Shape Measurements

Figure 17 shows the measured pressured scaled collisional broadening half-widths for NO and N_2 ($2\gamma_{NO-N2}$) over the temperature range 700 to 2100 K, and the power-law fit. The power-law fit gives a $2\gamma_{NO-N2}(T = 296)$ of 0.0679 and a temperature coefficient (n) of 0.69. HITEMP specifies these values at 0.049 and 0.6, respectively. The data in HITEMP and HITRAN was generated from measurements in air, which is approximately 78% N_2, 21% O_2, plus minor gases such as CO_2, Ar, etc. This accounts for the discrepancy between measured results and the HITEMP databases.

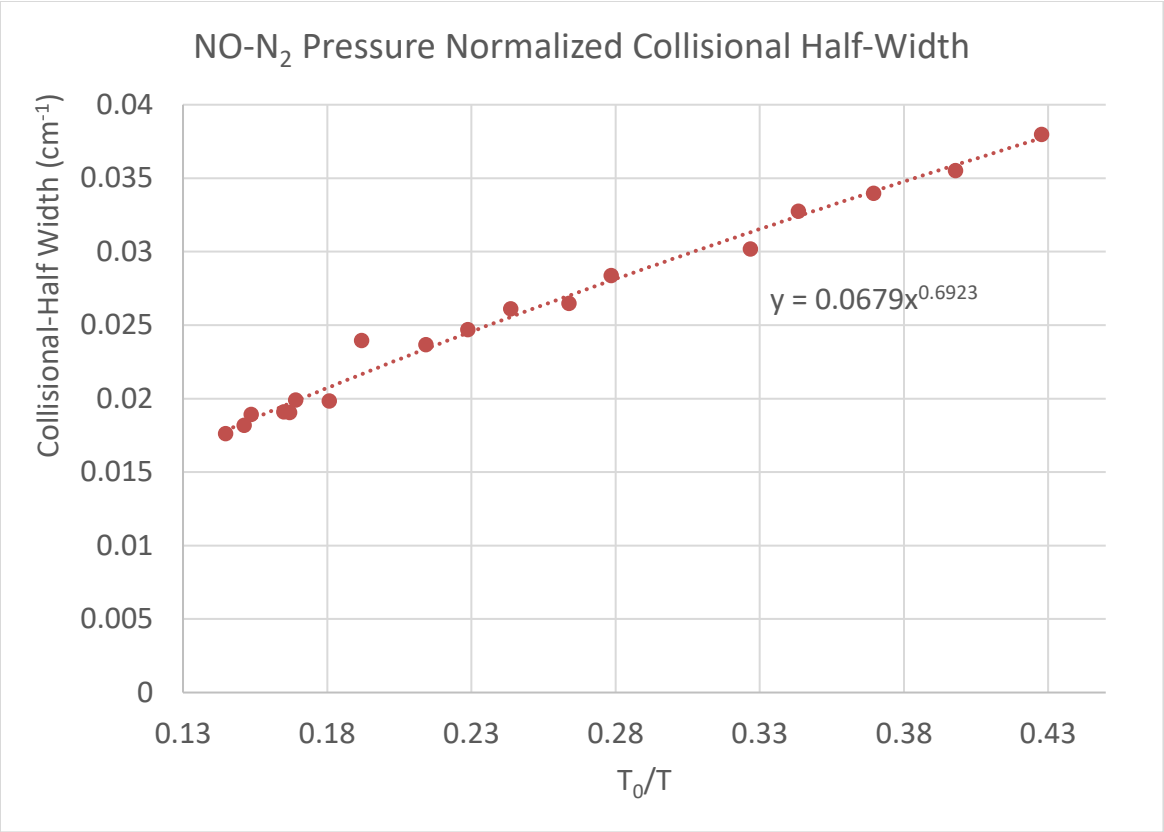

Figure 17: Measured pressure scaled collisional broadening half -widths of NO in N_2 from 700k to 2000K.

Figure 18 shows the measured pressured scaled collisional broadening half-widths for NO and CO_2 ($2\gamma_{NO-CO2}$) over the temperature range 700 to 2100 K, and the power-law fit. The power-law fit gives a $2\gamma_{NO-CO2}(T = 296)$ of 0.0586 and a temperature coefficient (n) of 0.40. The broadening due to N_2 is shown to be less than that of CO_2, which was expected.

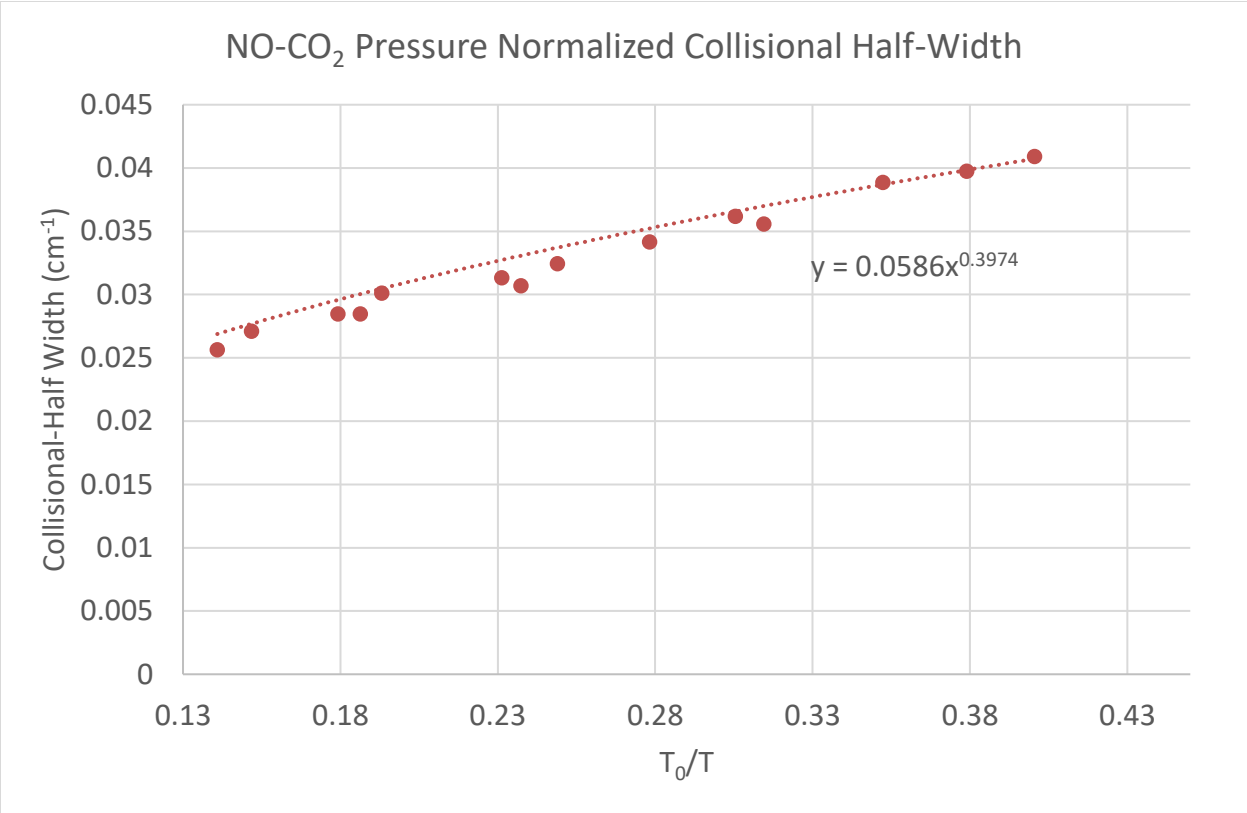

Figure 18: Measured pressure scaled collisional broadening half -widths of NO in CO_2 from 700k to 2000K.

CHAPTER 6: ABSORPTION SENSORS FOR COMBUSTION DEVICES

Success and Challenges of LAS for Practical Application

Laser absorption spectroscopy (LAS) is a powerful combustion diagnostic tool that permits the highly accurate, non-intrusive, and fast (MHz) evaluation of a system's thermodynamic state. LAS examines an analyte's spectra by actively probing with a laser to interrogate spectral absorption to infer properties, such as composition, temperature, pressure, and velocity. The great success of this technique has resulted in deployment in lab to investigate fundamental combustion physics and in the field for the development of novel combustion hardware or weapons platforms. As a field instrument for combustion or explosives diagnostics, additional challenges are not present in a lab's ideal conditions. A lot of consideration must be made in simply making the instrument portable enough to transport to the site without requiring considerable setup time. Optical access to the environment must be minimally intrusive and robust enough to handle the reactive flow's temperatures and pressures. Finally, the instrument needs to be coupled to the test facility or combustion hardware while maintaining a safe distance in case of a failure.

This chapter discusses the design approaches employed and lessons learned when developing LAS diagnostics for RDEs and high-explosives fireballs. These techniques were used in successful measurement campaigns at Southwest Research Institute, University of Alabama, and Eglin Air Force Research Base.

Field Deployable Instruments

A field-deployable instrument must be easily transportable, require minimal setup, and be insensitive to detuning from vibrations and shaking. Figure 19 shows a LAS developed to evaluate

CO_2, CO, H_2O, and temperature using four lasers, four mercury cadmium telluride (MCT) photovoltaic detectors, three fiber cables, a Bristol spectrometer, and 18+ optics. The optics are setup up on breadboards and placed in two acrylic boxes, one for the pitch and one for the catch, which protects the system during transport and allows the instrument to be purged with N_2. Purging the system mitigates interference from atmospheric gases and protects the electronics from humid air, which can cause condensation to form on some cooled components. While effective, this system contains many optical components, each of which contains at least four degrees of freedom that may become detuned or pose as a potential point of failure. Furthermore, when measuring at wavelengths that interact with H_2O, each optical component provides a surface for H_2O to condense and absorb. Purging the system greatly reduces the presence of H_2O, but H_2O does not just condense to surfaces; it makes a bond that does not break by simply desiccating the environment.

Optical systems can be sensitive to vibrations and acoustic noise, which are a significant byproduct in combustion and explosive systems. The best strategy for damping the system is placing it at a remote location on a heavy support structure or optical table, with a barricade between the combustion hardware and the instrument. However, these solutions are not always practical. The right side of Figure 19 shows solutions to an instrument that had to be placed within 2 m of an RDE. The instrument was placed on an optical breadboard and floated on air dampeners. The RDE produces acoustics similar to a small rocket engine, which can be picked up by the optical components. Egg crate foam was placed over the instrument enclosure to dampen the sound.

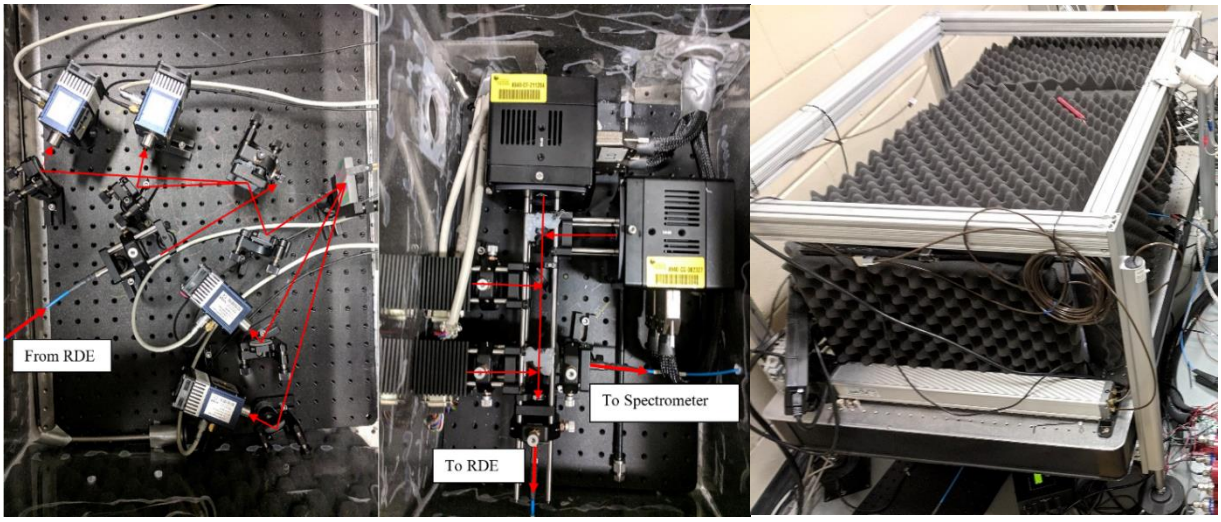

Figure 19: An example of a field-deployable LAS diagnostics system, which was used to evaluate detonative flows in an RDE.

Given the nature of combustion and weapon systems testing, it is common for facilities to be located outside and in remote locations. The electronics and optics must be protected from outside elements such as dust, humidity, and heat. As discussed previously, enclosing the instrument in helps protect it and allows the system to be purged with N2 or dry air. Temperature control can be much more challenging. Figure 20 shows the LAS diagnostics setup for outside measurements at Eglin Air Force Base (Florida) and Southwest Research Institute (Texas). For the measurements at Eglin, the instrument was placed inside an air-conditioned hut a couple of meters away from the test facility. However, at the end of each day, the system had to be removed and brought inside so it could be secured and safe from the weather. This posed significant logistical challenges as the system was large, heavy, and took some time to setup. The instrument deployed at SwRI was much more practical since the system was well contained in a single box and of manageable size.

Figure 20: Field instrumentation at Eglin Air Force Research Base (left) and Southwest Research Institute (right).

Optical Access to Combustion Hardware

An appealing aspect of optical-based diagnostics is the possibility of evaluating a flow system without disturbing or interacting with the physics, which few other techniques can offer. However, this comes at the cost of requiring some modification to the test facility to provide optical access. The optical access design is an important factor, which must consider flow dynamics, temperatures and pressures, instrument wavelengths, and harshness of the flow. There are two general approaches, a direct line of sight and probe.

A direct line of sight approach is the most common in which the laser beam is pitched directly across the test apparatus's channel or vessel. This method is favored as it does not interact with the fluid system but must conform to the test facility's geometry. Figure 21 shows window access points for a CH_4-air/O_2 fired RDE, which reached temperatures up to 3000 K and pressures of 6+ atm. Sapphire glass was used due to its desirable mechanical strength and transmissibility to

wavelengths up to 5μm. Despite sapphires mechanical properties, multiple glasses were blown during testing during strong detonation events, and over time the glass became etched, obscuring signal. Designing the plugs to be easily replaceable is critical to ensure an uninterruptable testing schedule.

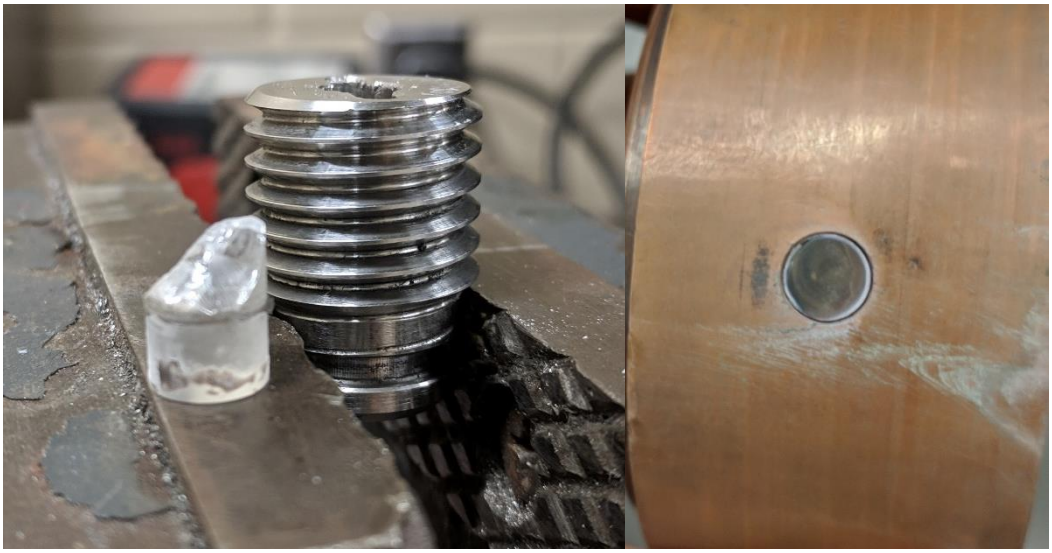

Figure 21: Windows for optical access to RDE detonation channel. (left) Window plug and shattered sapphire glass. (right) Etched sapphire glass on the inner surface access point.

Sometimes, the test facility's geometry does not permit a direct line of sight approach, so a probe is used, which penetrates the flow. With this method, control over the pathlength is gained, which is directly proportional to absorption. By minimizing the pathlength, the measurement approaches a point measurement and reduces losses from heavily particle ladened flows. Increasing the pathlength can increase sensitivity to species that may be in very low concentrations. However, this control's tradeoff is a perturbed flow that may impact the measurements or downstream evaluation of the flow. Since the LAS is line averaged measurement, the development of a boundary or shock wave could result in inaccurate assessments. Figure 22 shows a LAS probe

designed for evaluating temperature in fireballs at Eglin Air Force Base. The flow was highly energetic, particle ladened, and contained shrapnel. The optical ports were placed about 10 in. from the base to avoid the boundary layer region, and fins were attached to the probe's pillars to reduce the development of flow non-uniformities.

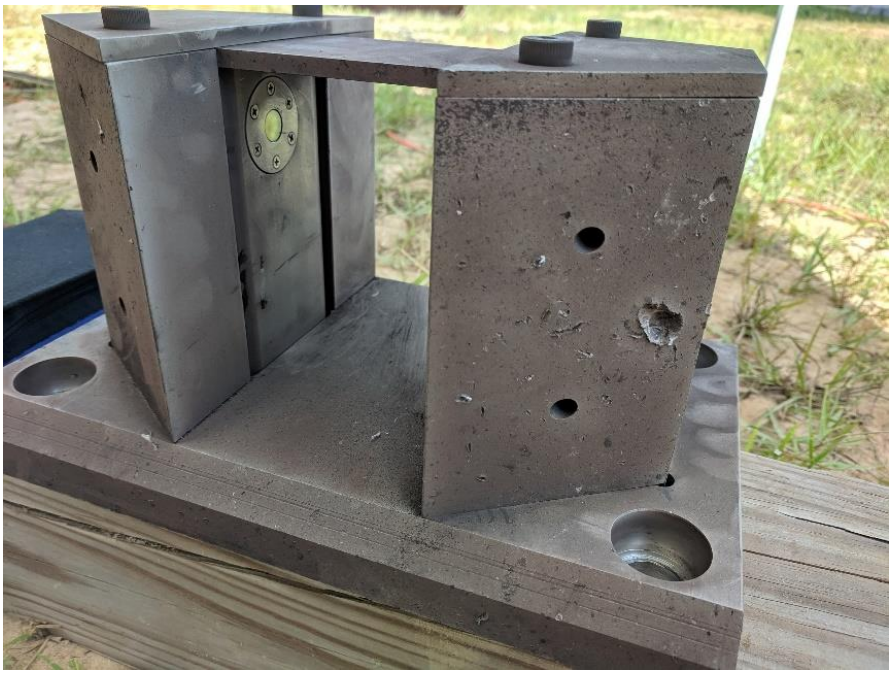

Figure 22: Probe for LAS measurements in fireballs. The probe was designed to withstand highly energetic flows and shrapnel.

Instrument to Facility Coupling

The LAS instrument can be coupled to the test facility or combustion hardware through free space, fiber couple, or direct mounting. Free space coupling laser diagnostics is not common outside the lab since it does not protect against misalignment, requires close proximity to the test apparatus, and allows the light to travel through uncontrolled space, which may affect measurements. As mentioned previously, the instrument should be placed as far away from the

hardware as possible since vibration and acoustic amplitude decreases proportionally to the square of the distance from the source. Fiber cables are highly valuable in allowing such placement and restrict the laser beam to only travel in controlled space.

When working in the near-infrared (NIR), silica fibers are available which are low-cost, flexible, and can transmit light over significant lengths (km). In the mid-infrared (MIR), fiber cables are limited to lengths of around 2 m, fragile, and more costly. Options in the MIR include hollow-silica-waveguides (HSW), indium fluoride (InF_3) and zirconium fluoride (ZrF_4), sapphire, and chalcogenide glass fibers. Depending on the specific wavelength and application, each material has advantages.

Figure 23 shows fiber cable coupling to an RDE at the University of Alabama. For these measurements, a chalcogenide single-mode fiber (SMF) was used to couple the pitch to RDE, and an InF_3 multi-mode fiber (MMF) was used to couple the RDE to the catch. MMF has a large core diameter and numerical aperture, which provides the lowest coupling losses. However, MMF incur spurious amplitude noise, called modal noise, that is affected by launch conditions, fiber flexure, and wavelength. This noise is caused by the different modes interacting within the waveguide, resulting in a speckled output that is spatially dynamic. These moving speckles result in amplitude fluctuation when the light is projected onto a photodiode that does have a spatially uniform response, which may include dirt or clipping of the fiber output. A solution to the modal noise problem is to use SMF, but this comes at the cost of significantly greater coupling losses.

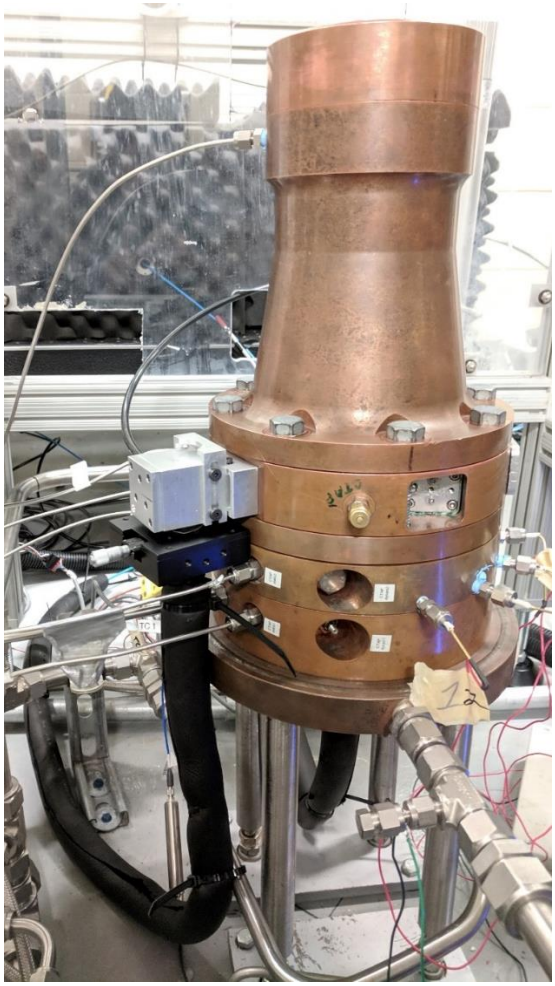

Figure 23: Fiber cable setup on a RDE at the University of Alabama. The fiber cables are sheathed in black foam to protect them from thermal and mechanical stress. The pitch fiber is a single-mode chalcogenide fiber that is attached to the outer diameter of the RDE. The catch fiber is a InF_3 fiber that is routed through the center of the RDE.

The last option is to directly mount the instrument onto the test facility or combustion hardware, such is shown in Figure 24. Figure 24 shows a probe designed to measure the exhaust of a gas turbine combustor. A fiber couple caries the signal to the probe but the photovoltaic detectors are directly mounted on the probe, which bypasses the need for a catch fiber and reduces loss and noise. In this example, only the receiving equipment is mounted on the hardware, but it is conceivable to mount the source directly. Solid-state lasers such as QCL are extremely small,

with the bulk of their mass being a heat sink. The challenge is mounting a multiplexed system, but there are low mass solutions to this problem [13].

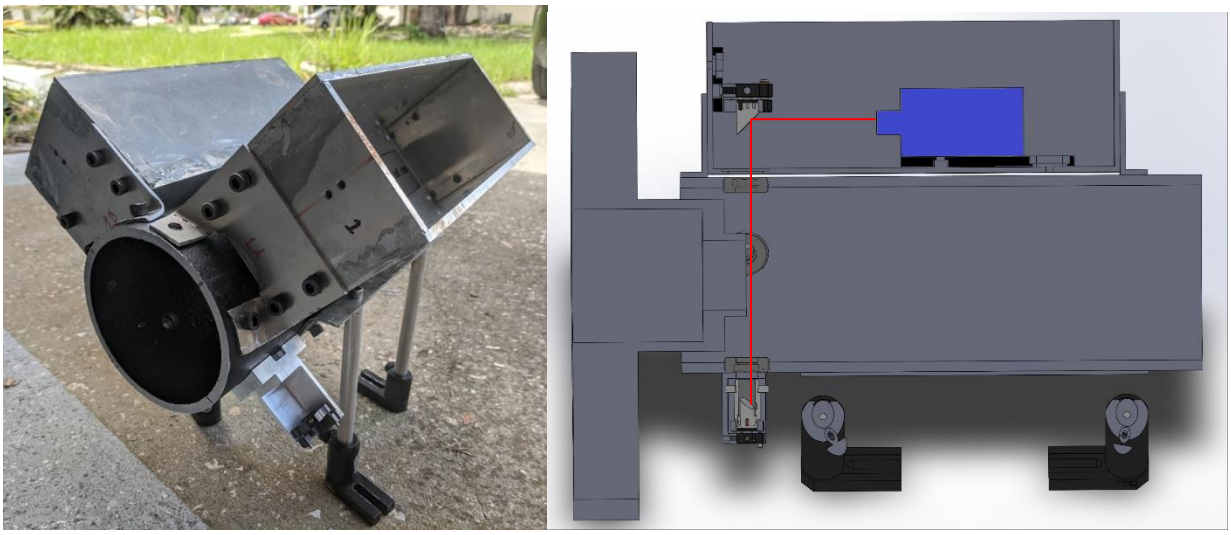

Figure 24: Exhaust probe demonstrating direct mounting. (left) Actual hardware constructed from 4" steel pipe. (right) Cross-sectional view from CAD rendering showing a line-of-sight path.

Summary

Bringing laser diagnostic to the field often requires a long lead up to the measurement campaign with only a short window to acquire the data. Therefore, it is critical to design field instruments around failure mitigation and to reduce downtime. The reoccurring theme of the designs and lessons learned discussed in this chapter is to reduce complexity. It is easy to deprioritize or neglect these design criteria, but setup time and failure modes should be at the top of the list.

CHAPTER 7: TEMPERATURE AND H2O MEASUREMENTS IN RDE DETONATION CHANNEL

Introduction

The University of Central Florida (UCF) set out to develop an instrument capable of measuring total pressure within the detonation chamber of a Rotating Detonation Engine (RDE). The total pressure is a function of static pressure (P), static temperature (T), gas composition (x_i), and flow velocity (u_i) and may be expressed using equations 15 and 16 below. The major products of combustion are H_2O, CO_2, and CO for an engine running on CH_4-air. A Tunable Diode Laser Absorption Spectroscopy (TDLAS) instrument was developed to resolve these major products and static temperature. Velocity was resolved through Particle Imaging Velocimetry (PIV). In addition to these laser-based instruments, high-speed (MHz) piezoelectric pressure transducers (PCB Piezotronics) provide static pressure (P) measurements that complete the equation for total pressure.

$$P_0 = P\left(\frac{T_0}{T}\right)^{\frac{\gamma(x_i)}{\gamma(x_i)-1}} \tag{15}$$

$$\frac{T_0}{T} = \left(1 + \frac{u_\theta^2 + u_Z^2}{2C_p(x_i)T}\right) \tag{16}$$

The bulk of UCF's efforts was to produce measurements of static temperature, H_2O, CO_2, and CO using TDLAS within the detonation chamber of an RDE at MHz rates. Previous attempts at measuring temperature and gas composition within an RDE's flow have been limited to a bandwidth no greater than 100kHz. These past efforts made use of techniques that scanned or modulated the lasers' wavelength to collect more spectral information, reduce uncertainty, and

reject background noise. However, tuning of the wavelength comes at the cost of temporal resolution. To achieve MHz rates, we employed a fixed-wavelength, direct absorption approach, and used hardware to minimize noise and uncertainty.

System Design

For the instrument discussed here, two wavelengths were selected: 2.55μm, which has a high sensitivity to water at low temperatures, and 2.48μm, which has peak sensitivity around 1300K. Figure 25 shows the temperature sensitivity curves for these two wavelengths. The RDE is expected to operate between 2000 to 3000K, so each wavelength's absorbance should be inversely proportional to temperature.

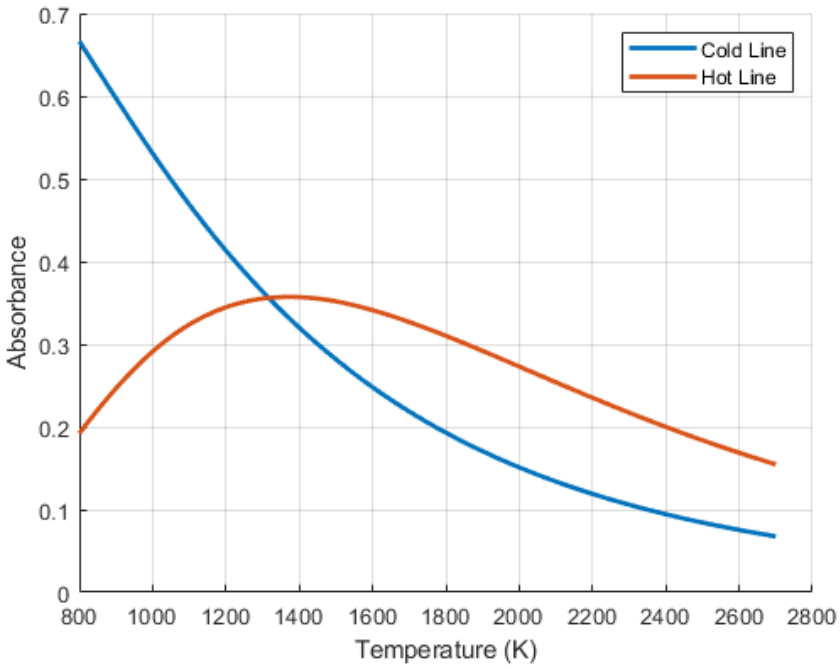

Figure 25: The temperature response curve for the two selected water lines. The "hot line" (2.48μm) is more sensitive to higher temperatures than the "cold line" (2.55μm).

In this case, fixed-wavelength, direct absorption is used (not scanned), so the ratio is also dependent on static pressure and weakly on gas composition, which is pictured in Figure 26 below. An initially assumed equilibrium gas concentration is used to resolve static temperature, and static pressure from the pressure transducers is provided. With the calculated static temperature, water concentration is calculated from each wavelength. This process is iterated until the two water concentrations converge.

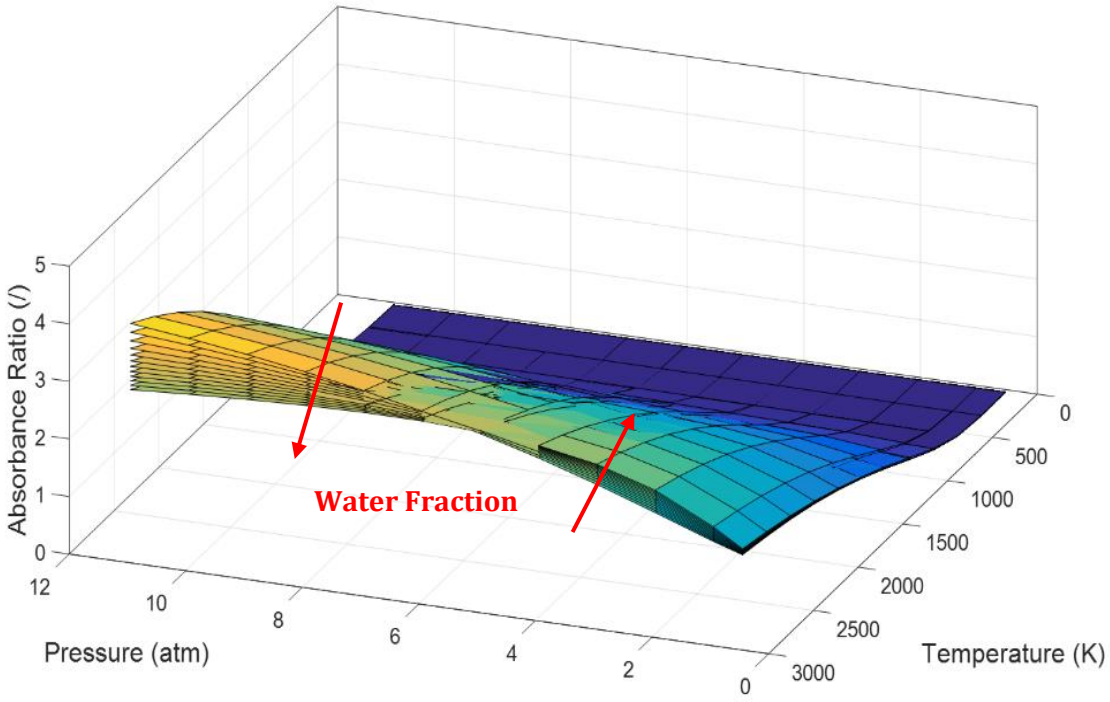

Figure 26: The absorbance ratios of the two wavelengths used to measure water and temperature. For operation under 8 atm, this function is weakly dependent on gas composition.

The TDLAS sensor incorporates four lasers at four wavelengths: two targeting water (2551 nm and 2482 nm), one targeting CO_2 (4250nm), and one targeting CO (4580 nm). The four wavelengths are combined using three beam splitters then demultiplexed using diffraction gratings. The lasers are routed to the engine using a single-mode, chalcogenide glass fiber cable

connected to the RDE through a sapphire window on the outer diameter. The signal is transmitted through the 1 cm annular detonation channel and received through a second window on the engine's inner body, then coupled into a second optical fiber. Each wavelength has a dedicated Mercury Cadmium Telluride (MCT) photovoltaic (PV) detector. This arrangement is shown in Figure 27.

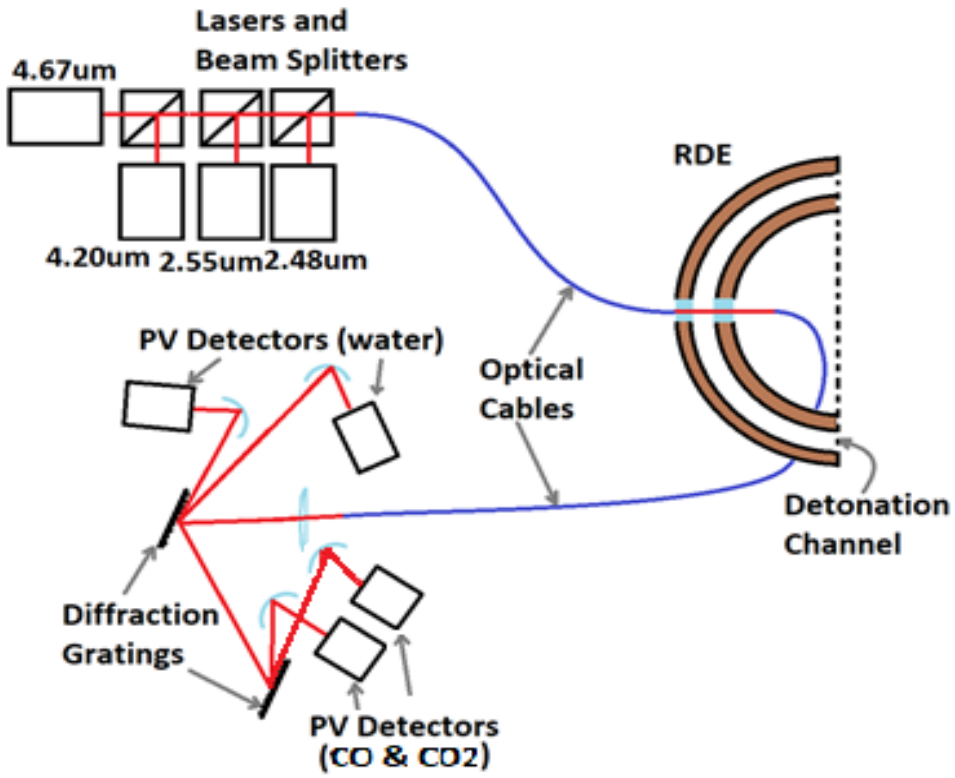

Figure 27: TDLAS configuration for water and temperature measurements in an RDE.

Figure 28 shows the interface between the TDLAS instrument and the RDE hardware. The aluminum block houses an off-axis parabolic mirror, which reduces misalignment from beam steering. The black block attached to it allows the fine-tuning of the instrument. Making the measurements within the detonation channel helps ensures a uniform line-of-sight

measurement. Previous measurements made in the detonation channel utilized the NIR region and a double pass due to the wavelength band's lower absorption strength. As done by our team, using the MIR region provides strong absorption, allowing high sensitivity with a single pass, which reduces beam steering effects.

Figure 28: Custom interface for TDLAS and RDE hardware.

After measurements were made in 2017 at Southwest Research Institute (SwRI), several observations were made on the instrument's performance, and improvements were implemented for continued testing in 2018. With the RDE's unique flow and high operating frequency, a comprehensive evaluation of the instrument before measurements was challenging. The instrument was evaluated using the UCFs high-pressure shock tube, which replicates some of the conditions within an RDE but not the fast repetition rate and complex flow. The SwRI measurements gave us a great deal of insight into how to accommodate the challenging

environment of the RDE better. Figure 29 shows a side by side comparison of the 2017 system (left) and the improved 2018 system (right). The enhanced system was fitted with active and passive damping, acoustic damping, single-mode fibers, and a custom interface for the RDE (Figure 28).

Figure 29: Side by side comparison of the SOTA measurement system I (left) and II (right).

Improvements to the structural support and the addition of active damping to the system reduce the mechanical vibration transmitted to the optics from the systems' operation. While the vibrations' frequency is much lower than the engine's operating frequency and, therefore, filtered out by cycle averages, these vibrations could affect baseline signal measurements or misalign optics. The improvements eliminated the need to realign the optics with the pitch and catch subsystems, which reduced downtime.

During the 2018 measurements at UA, one of the multi-mode fibers was replaced with single-mode fiber. Modal-noise in fiber cables is formed when bending stress causes the index of refraction variations along the cable radius, which reduces spatial coherence. The single-mode fiber is effective by filtering out higher-order modes but can attenuate the laser source. Modal noise was a considerable problem in the measurements made at SwRI, so the tradeoff was acceptable. Furthermore, we were able to recover our signal loss from the single-mode fiber with our custom RDE/TDLAS interface.

A significant source of difficulty during the 2017 SwRI measurements was coupling the TDLAS instrument to the RDE. For this, we used an off the shelf Thorlabs flange lens, which had a few flaws that made it extremely difficult to tune and became misaligned after the engine fired. To address this, we developed a new interface, which is shown in Figure 27. This new interface used an off-axis parabolic mirror, which is more appropriate for the large spectral ranges that we are using. Additionally, it has a larger numerical aperture and a longer focal length for a nearly paraxial design even during beam steering. The tuning on the interface is much finer with greater range, making it much simpler and quicker to couple the instrument to the RDE. On top of this, signal strength was significantly improved. An overhead shot of the final system is shown in Figure 30 below.

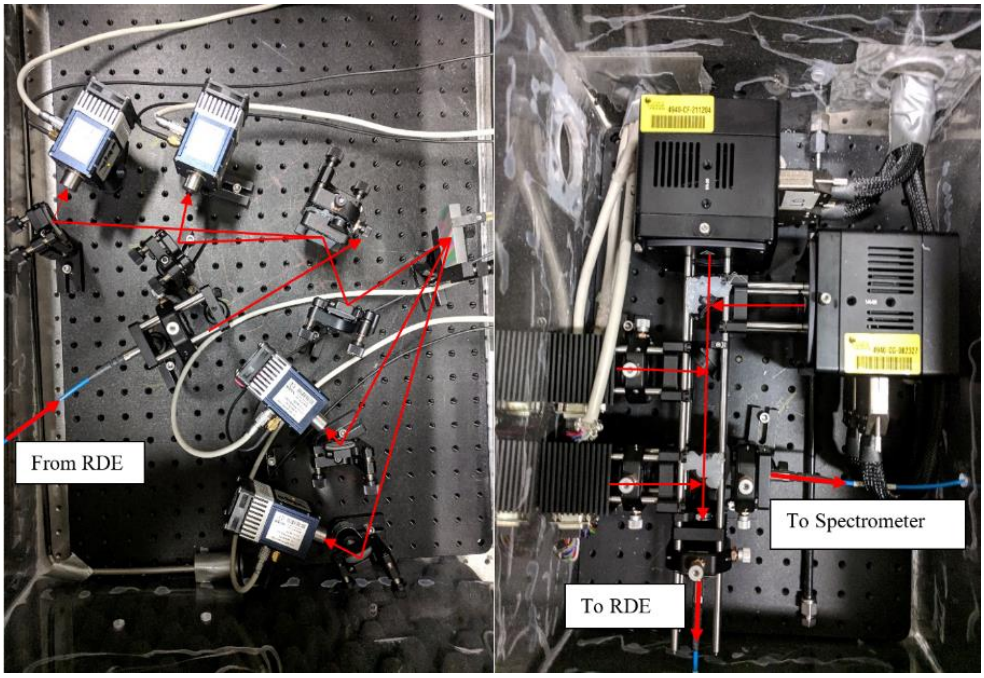

Figure 30: An overhead view of the 2018 TDLAS instrument. The pitch system is on the right, containing the four lasers multiplexed through three beam splitters and sent to the RDE using single-mode fiber. A second fiber is used to send the signal to a spectrometer. The left side shows the catch system where the four wavelengths are demultiplexed and measured with MCT detectors.

Results

The table below summarizes our accomplishments over the past two years. UCF made measurements in the detonation chamber of an H_2-O_2/air fuel engine at SwRI in 2017 and a CH_4-O_2/air fueled engine at UA in 2018 [14, 15]. The 2017 SwRI measurements also include Particle Imaging Velocimetry (PIV) measurements in the exhaust plane of the RDE [16]. The enhanced TDLAS instrument showed great improvement from the previous year. The custom RDE/TDLAS interface significantly increased signal strength and reduced the amount of time it took to couple to the engine. Noise levels were reduced, which allowed us to capture fast features that can also be seen in the high-speed pressure measurements.

Table 1: Summary of UCF RDE diagnostics accomplishments.

Year One Accomplishments	**Year Two Accomplishments**
SOTA System Procurement & Assembly	SOTA System I to II Design
SOTA System Validation Testing	SOTA System II Procurement and Assembly
SOTA System Testing at SwRI	SOTA Measurement System II Assessment
Two 54th Joint Propulsion Conference Papers	SOTA Measurement System II Testing at UA
	2019 AIAA SciTech Conference Paper

Temperature and water measurements were successfully made within Aerojet Rocketdyne's 10cm RDE at the University of Alabama in November of 2018 using the UCF TDLAS. Attempts were made to measure CO and CO_2, but difficulties were encountered in simultaneously aligning all four lasers through the RDE. It was decided to revisit these measurements after temperature and water measurements were completed with the limited time available, if time permitted. The RDE was fueled with CH_4 and O_2 enriched air with an equivalence ratio near one. The RDE was equipped with a diffuser and nozzle designed to condition the flow while minimizing viscous losses. Three backpressure nozzles were available, allowing for a range of constriction at the exit. During the window open for TDLAS measurements, there were many difficulties getting the engine to enter stable operation with a well-formed rotating detonation wave (RDW). Instead, the engine would deflagrate with no discernable operating mode picked up by the ion probes or PCBs. Stable operation was achieved on the smallest nozzle with a mass flow rate of 0.679lbm/s. An attempt to obtain a stable operating point for the largest backpressure nozzle was made, but higher flow rates were necessary, which resulted in the outer window fracturing

and the single-mode fiber becoming damaged. The damaged fiber was not easily replaceable, so it ended any further efforts.

A sample of the raw data for the two wavelengths (2.48μm and 2.55μm) used to measure water, and the static temperature is shown in Figure 31, which was sampled at 5MHz. Static pressure was evaluated by combining CTAP and PCB measurements. The PCB was clocked about 50° clockwise from the TDLAS access window. Measurements were taken at the end of the detonation chamber, just before the flow enters the diffuser. Therefore, it was expected the instrument would pick up the oblique shock and detonation products. For the current discussion, the engine was operated with the conditions specified in Table 2.

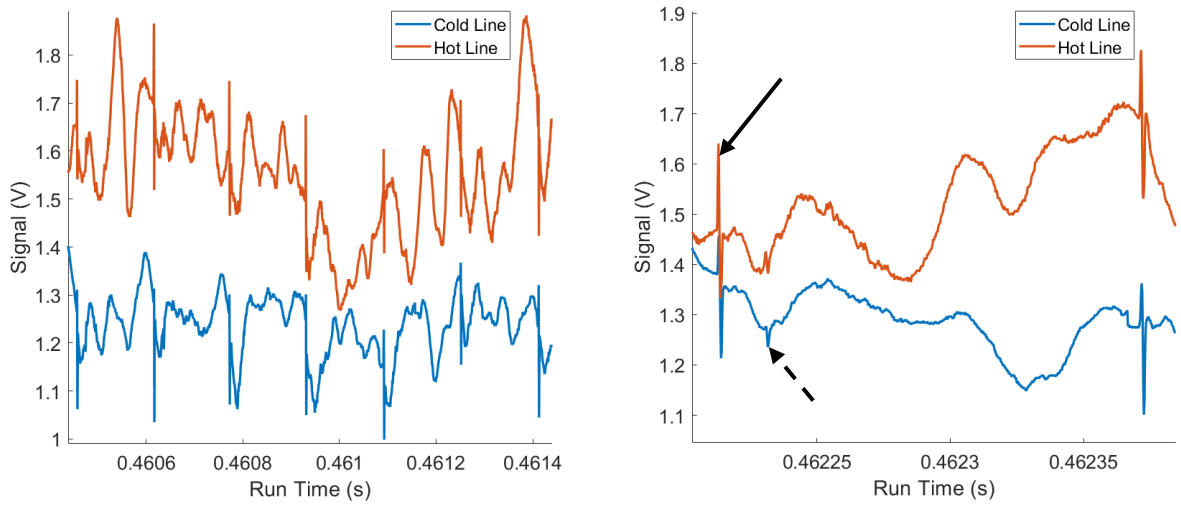

Figure 31: A sample of raw TDLAS data for the discussed results. The left shows six cycles of the RDW punctuated by a sharp spike (Schlieren spike). The right shows a single cycle that makes a secondary Schlieren spike (dotted arrow) observable, which coincides with the second pressure peak. The cold line is the 2.55μm wavelength laser and the hot line is the 2.48μm wavelength laser.

Table 2: Operating conditions for the discussed results. Mass flow rates are in lbm/s.

ϕ	$\dot{m}_{CH4}$	$\dot{m}_{air}$	$\dot{m}_{O2}$	$\dot{m}_{total}$	Nozzle
1.03	0.103	0.225	0.351	0.679	#1

A few notable features are observable in the raw data that should be noted before the results are discussed. First, there is an apparent oscillation at a frequency of about 1.2kHz in the TDLAS signals, which is slower than the engine's operation (approx. 6.3kHz). On closer inspection, it can be seen that the response of each laser changes with oscillation as well. That is, during some period, each wavelength has a roughly positively proportional response to the other, while in the following period, their responses are inverse of one another. This may be seen on the left side of Figure 31, where this inversion takes place during the second cycle. As shown in Figure 25, this inverse response should only occur at a temperature below approximately 1880F (1300K), which is considerably lower than expected.

Additionally, the signals continue their current trend with minimal discontinuity after the oblique shock passes (marked by the Schlieren spike). This suggests the shock is wave may be weak and that there is minimal state change (temperature or water formation/disassociation). Finally, if the raw data is zoomed-in onto a single cycle, as shown on the right side of Figure 31, a second Schlieren spike is observed. These spikes occur when sharp thermodynamic gradients occur along the beam path, such as with the oblique shock, resulting in the laser being deflected. The origins of this secondary spike are discussed following the presented results.

Figure 32 shows the results for the discussed flow conditions and nozzle configuration. The left side shows static temperature and water mole fraction, as measured by the UCF TDLAS, and the right side shows static pressure, as measured by CTAP and PCB. A noted previously, there is an overlapping cycle that appears to correspond to the flow briefly dropping below 1880F. During this period, the TDLAS has a different response than higher temperature flows. Since the data is cycle averaged, the "low-temperature cycles" were ignored since averaging them with the "high-temperature cycles" resulted in difficult to interpret data since they are inverse of one another for the "hot line." This was done by checking the concavity of the first peak in the cycle and the coherence each wavelength has with the other. Consequently, the results presented should be considered the high-temperature end for this flow condition.

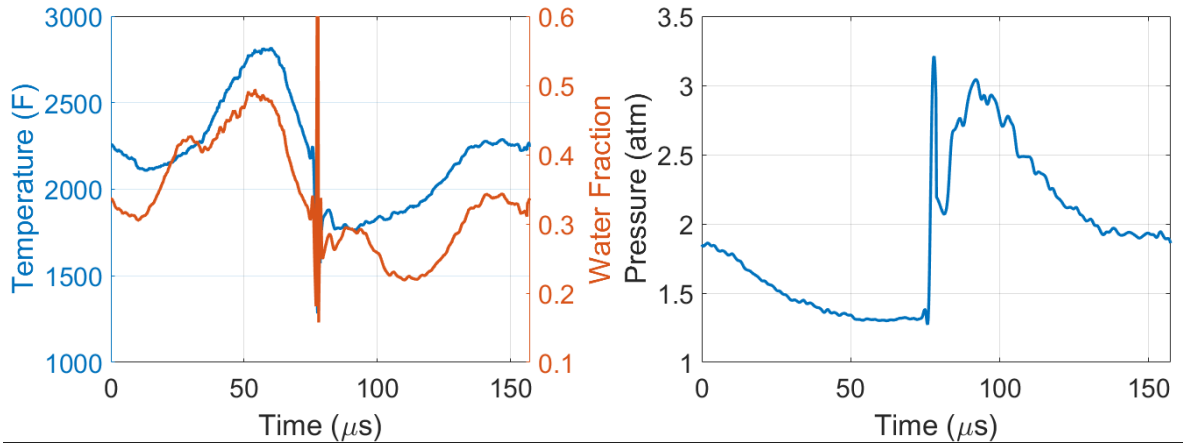

Figure 32: TDLAS measurement results (left) and static pressure measurements (right). The cycle averaged data has been centered so that the oblique shock wave occurs midway through the plot (~79μs).

Examining the temperature profile in Figure 32, the temperature declines just before the oblique shock arrives and then stalls briefly after it passes. It then begins to rise, where it peaks ~20μs before the shock wave arrives. At first, this seemed counter to expected, with the peak

temperature anticipated to occur around the peak pressure. However, a clear picture begins to emerge after putting together the raw data's details, the low operating temperature, and the overall difficulty obtaining a stable RDW. It is apparent that incomplete combustion occurs within the RDW stage, and the remaining reactants are combusting after passing through the oblique shock wave. The secondary Schlieren spike likely corresponds to this combustion event. As the gas expands after the shock wave, the reaction continues, resulting in temperature rise and water formation.

Ongoing and Future Work

The hardware we have developed in partnership with Aerojet Rocketdyne will serve as a foundation for our ongoing work into RDEs, propulsion, and power generating hardware. As we have outlined, producing measurements at MHz rates in high temperature and pressure dynamic range flows is new grounds and extremely challenging. Techniques have been developed, which greatly reduce noise and uncertainty by sweeping and modulating the lasers' wavelength used to probe the gases. However, scanning the wavelength comes at the cost of acquisition speed. In our ongoing work, we plan to use a fixed-wavelength direction-absorption-spectroscopy (fixed-DAS) technique that has been hardened for the high vibrations produced by RDEs and supplements it with scanned-wavelength wavelength-modulation-spectroscopy (scanned-WMS). This technique will capture the fast features of the RDEs while maintaining the high SNR necessary for advancing research to the next stage of development. This is analogous to how high-speed static pressure measurements are made using PCB pressure transducers. The PCB pressure transducers experience thermal drift during hot gas measurements, so supplementary Capillary Tube Averaged

Pressure (CTAP) measurements are taken at a slower rate to correct the PCB measurements' baseline.

Vasu Labs has developed a range of diagnostics used to investigate fundamental studies in combustion, power, and propulsion, including fast CO temperature measurements [17, 18], organophosphate compounds [19-21], and hydrocarbons [22-25]. Our partnership with labs at UCF's College of Optics and Photonics, CREOL, allows us to develop novel laser-based diagnostics that push the state of the art's boundaries. This includes the recent development of an acousto-optically modulated quantum cascade laser (AOM-QCL), which provides rapid switching between wavelength bands for static temperature or selective species measurements [17, 18]. New diagnostics are in development, which will allow the measurement of different emission gases such as NOx. Our facilities include high-pressure shock tubes and a flat flame burner, supporting us in evaluating new diagnostic techniques from 0.1-100bar and 300-5000K.

REFERENCES

1. Goldenstein, C. S., Almodóvar, C. A., Jeffries, J. B., Hanson, R. K., and Brophy, C. M. "High-bandwidth scanned-wavelength-modulation spectroscopy sensors for temperature and H2O in a rotating detonation engine," *Measurement Science and Technology* Vol. 25, No. 10, 2014, p. 105104.

2. Rein, K. D., Roy, S., Sanders, S. T., Caswell, A. W., Schauer, F. R., and Gord, J. R. "Measurements of gas temperatures at 100 kHz within the annulus of a rotating detonation engine," *Applied Physics B* Vol. 123, No. 3, 2017.

3. Rein, K. D., Roy, S., Hoke, J., Caswell, A. W., Schauer, F., and Gord, J. R. "Multi-beam Temperature Measurements in a Rotating Detonation Engine Using H2O Absorption Spectroscopy," *55th AIAA Aerospace Sciences Meeting*, 2017.

4. Rothman, L. S., Gordon, I. E., Babikov, Y., Barbe, A., Chris Benner, D., Bernath, P. F., Birk, M., Bizzocchi, L., Boudon, V., Brown, L. R., Campargue, A., Chance, K., Cohen, E. A., Coudert, L. H., Devi, V. M., Drouin, B. J., Fayt, A., Flaud, J. M., Gamache, R. R., Harrison, J. J., Hartmann, J. M., Hill, C., Hodges, J. T., Jacquemart, D., Jolly, A., Lamouroux, J., Le Roy, R. J., Li, G., Long, D. A., Lyulin, O. M., Mackie, C. J., Massie, S. T., Mikhailenko, S., Müller, H. S. P., Naumenko, O. V., Nikitin, A. V., Orphal, J., Perevalov, V., Perrin, A., Polovtseva, E. R., Richard, C., Smith, M. A. H., Starikova, E., Sung, K., Tashkun, S., Tennyson, J., Toon, G. C., Tyuterev, V. G., and Wagner, G. "The HITRAN2012 molecular spectroscopic database," *Journal of Quantitative Spectroscopy and Radiative Transfer* Vol. 130, 2013, pp. 4-50.

5. Letchworth, K. L., and Benner, D. C. "Rapid and accurate calculation of the Voigt function," *Journal of Quantitative Spectroscopy and Radiative Transfer* Vol. 107, No. 1, 2007, p. 173.

6. Humlíček, J. "Optimized computation of the voigt and complex probability functions," *Journal of Quantitative Spectroscopy and Radiative Transfer* Vol. 27, No. 4, 1982, p. 437.

7. Drayson, S. R. "Rapid computation of the Voigt profile," *Journal of Quantitative Spectroscopy and Radiative Transfer* Vol. 16, No. 7, 1976, p. 611.

8. Rothman, L., Gordon, I., Barber, R., Dothe, H., Gamache, R., Goldman, A., Perevalov, V., Tashkun, S., Tennyson, J. J. J. o. Q. S., and Transfer, R. "HITEMP, the high-temperature molecular spectroscopic database," Vol. 111, No. 15, 2010, pp. 2139-2150.

9. Mulvihill, C. R., Alturaifi, S. A., and Petersen, E. L. "High-temperature He- and O2-broadening of the R(12) line in the 1←0 band of carbon monoxide," *Journal of Quantitative Spectroscopy and Radiative Transfer* Vol. 217, No. J Chem Phys 78 1983, 2018, pp. 432-439.

10. Zhou, X., Liu, x., Jeffries, J. B., and Hanson, R. K. "Development of a sensor for temperature and water concentration in combustion gases using a single tunable diode laser," *Measurement Science and Technology* Vol. 14, 2003.

11. Rutkowski, L., Foltynowicz, A., Schmidt, F. M., Johansson, A. C., Khodabakhsh, A., Kyuberis, A. A., Zobov, N. F., Polyansky, O. L., Yurchenko, S. N., and Tennyson, J. "An experimental water line list at 1950 K in the 6250–6670 cm − 1 region," *Journal of Quantitative Spectroscopy and Radiative Transfer* Vol. 205, 2018, pp. 213-219.

12. Schwarm, K. K., Dinh, H. Q., Goldenstein, C. S., Pineda, D. I., and Spearrin, R. M. "High-pressure and high-temperature gas cell for absorption spectroscopy studies at wavelengths up to 8 μm," *Journal of Quantitative Spectroscopy and Radiative Transfer*, No. Progress in Energy and Combustion Science 60 2017, 2019.

13. Loparo, Z., Thurmond, K., Lyakh, A., and Vasu, S. "Novel diagnostic technique for ultra-fast, simultaneous temperature and concentration measurements for harsh hypersonic flows," *23rd AIAA International Space Planes and Hypersonic Systems and Technologies Conference*. 2020.

14. Thurmond, K., Vasu, S., Stout, J., Coogan, S. B., Ahmed, K. A., Dunn, I. B., White, S., and Nolen, C. "MHz-rate Laser Spectroscopic Instrument for Reacting Flow Composition and Temperature Measurements inside Rotating Detonation Engines (RDEs)," *2018 Joint Propulsion Conference*. 2018.

15. Thurmond, K., Dunn, I., Ahmed, K. A., and Vasu, S. "Measurements of H2O, CO2, CO, and static temperature inside rotating detonation engines," *AIAA Scitech 2019 Forum*. 2019.

16. Dunn, I. B., Thurmond, K., Ahmed, K. A., and Vasu, S. "Exploration of Measuring Pressure Gain Combustion within a Rotating Detonation Engine," *2018 Joint Propulsion Conference*. 2018.

17. Loparo, Z. E., Muraviev, A. V., Figueiredo, P., Lyakh, A., Peale, R. E., Ahmed, K., and Vasu, S. S. J. J. o. E. R. T. "Shock Tube Demonstration of Acousto-Optically Modulated Quantum Cascade Laser as a Broadband, Time-Resolved Combustion Diagnostic," Vol. 140, No. 11, 2018, p. 112202.

18. Loparo, Z. E., Ninnemann, E., Thurmond, K., Laich, A., Azim, A., Lyakh, A., and Vasu, S. S. J. O. l. "Acousto-optically modulated quantum cascade laser for high-temperature reacting systems thermometry," Vol. 44, No. 6, 2019, pp. 1435-1438.

19. Neupane, S., Barnes, F., Barak, S., Ninnemann, E., Loparo, Z., Masunov, A. m. E., and Vasu, S. S. J. T. J. o. P. C. A. "Shock tube/laser absorption and kinetic modeling study of triethyl phosphate combustion," Vol. 122, No. 15, 2018, pp. 3829-3836.

20. Neupane, S., Loparo, Z., Barak, S., Pryor, O., Ninnemann, E., and Vasu, S. "MHz-Rate Measurements of Time-Resolved Species Concentrations in Shock Heated Chemical Weapon Simulants," *2018 IEEE Research and Applications of Photonics In Defense Conference (RAPID)*. IEEE, 2018, pp. 1-4.

21. Neupane, S., Peale, R., and Vasu, S. J. J. o. M. S. "Infrared absorption cross sections of several organo-phosphorous chemical-weapon simulants," Vol. 355, 2019, pp. 59-65.

22. Koroglu, B., Neupane, S., Pryor, O., Peale, R. E., Vasu, S. S. J. J. o. Q. S., and Transfer, R. "High temperature infrared absorption cross sections of methane near 3.4 μm in Ar and CO2 mixtures," Vol. 206, 2018, pp. 36-45.

23. Koroglu, B., Pryor, O. M., Lopez, J., Nash, L., Vasu, S. S. J. C., and flame. "Shock tube ignition delay times and methane time-histories measurements during excess CO2 diluted oxy-methane combustion," Vol. 164, 2016, pp. 152-163.

24. Loparo, Z. E., Lopez, J. G., Neupane, S., Partridge Jr, W. P., Vodopyanov, K., Vasu, S. S. J. C., and Flame. "Fuel-rich n-heptane oxidation: A shock tube and laser absorption study," Vol. 185, 2017, pp. 220-233.

25. Pryor, O., Barak, S., Lopez, J., Ninnemann, E., Koroglu, B., Nash, L., and Vasu, S. J. J. o. E. R. T. "High pressure shock tube ignition delay time measurements during oxy-methane combustion with high levels of CO2 dilution," Vol. 139, No. 4, 2017, p. 042208.